13 Ultramafic Cumulates of Oceanic Affinity in an Intracontinental Subduction Zone: Ultrahigh-Pressure Garnet Peridotites from Pohorje (Eastern Alps, Slovenia)

Jan C.M. De Hoog[1], Marian Janák[2], Mirijam Vrabec[3] and Keiko H. Hattori[4]

[1]School of GeoSciences, The University of Edinburgh, Edinburgh, UK
[2]Geological Institute, Slovak Academy of Sciences, Bratislava, Slovak Republic
[3]Department of Geology, University of Ljubljana, Ljubljana, Slovenia
[4]Department of Earth Sciences, University of Ottawa, Ottawa, ON, Canada

13.1 Introduction

Continental subduction and exhumation have been recognized as processes common to continental collision, which has led to the widespread occurrence of ultrahigh-pressure (UHP) metamorphosed rocks in collision belts (Chopin, 2003). Garnet peridotites are subordinate but common constituents in nearly all UHP terranes. They are classified as crustal or mantle derived depending on their emplacement within the crust prior to or during continental subduction (Brueckner & Medaris, 2000). The origin of peridotites is diverse and includes ultramafic cumulates and residual mantle of subcontinental, oceanic, or sub-arc mantle affinity. Identification of this origin is not always straightforward due to complex, often multiphase metamorphic histories, but these rocks may provide important information about the geodynamic and premetamorphic history of their host terranes (Carswell, 1986; Brueckner & Medaris, 2000).

The Pohorje Mountains in northeast Slovenia represent the southernmost and most deeply subducted part of a large area of subducted continental crust that includes the Koralpe and Saualpe regions (Kurz & Fritz, 2003; Janák et al., 2004, 2006, 2009; Schmid et al., 2004; Bruand et al., 2010). The Pohorje region is mainly

composed of continental crust (gneisses, schists, amphibolites, and marbles) but in the southeastern part it contains a large ultramafic complex of predominantly depleted harzburgites (Slovenska Bistrica Ultramafic Complex, SBUC) with kyanite eclogites and garnet peridotites (Hinterlechner-Ravnik et al., 1991; Janák et al., 2004, 2006; Miller et al., 2007; De Hoog et al., 2009; Kirst et al., 2010). The geochemistry of the mafic and ultramafic rocks points to an oceanic affinity (Sassi et al., 2004; Miller & Konzett, 2005; De Hoog et al., 2009), but their origin remains unsolved. Janák et al. (2006) proposed a model in which garnet peridotites were incorporated from the overlying mantle during subduction. De Hoog et al. (2009) adopted this model and extended it to the whole SBUC, but proposed an alternative scenario where mantle is derived from continental rifting during the Permian. The latter model is preferred by Kirst et al. (2010) based on the structural position of the SBUC. Also, the protolith of the garnet peridotites has not been firmly established. Janák et al. (2006) suggested that the protolith was depleted peridotite later metasomatized by melts, but an ultramafic cumulate origin was proposed by Janák et al. (2008). The main purpose of this paper is to determine the protolith and tectonic affinity of the garnet peridotites, to constrain their relationship with the depleted mantle rocks of the SBUC, and to discuss implications for the geodynamic history of the Pohorje region.

13.1.1 Tectonic and Geological Background

Ultramafic rocks occur in the southeasternmost part of the Pohorje Mountains near Slovenska Bistrica (Figure 13.1), where they form a continuous body of ~8 × 1 km size (SBUC; Janák et al., 2006). It is composed of strongly serpentinized harzburgites and subordinate dunites, garnet peridotites, and pyroxenites (Hinterlechner-Ravnik et al., 1991; Janák et al., 2006; De Hoog et al., 2009; Kirst et al., 2010), and also contains small lenses, boudins, and bands of partially amphibolitized eclogites. Garnet-free coronitic metatroctolites were reported by Hinterlechner-Ravnik et al. (1991). Large kilometer-size eclogite bodies occur at the contact of the SBUC with overlying country rocks (Figure 13.1). MORB-like trace-element signatures of eclogites were interpreted by Visona et al. (1991) in terms of an origin within the oceanic floor. The oceanic affinity of mafic units was confirmed in further work by Sassi et al. (2004) and Miller et al. (2005, 2007). An oceanic origin was also proposed for the SBUC based on its similarity to depleted abyssal peridotites (De Hoog et al., 2009).

The country rocks enclosing the SBUC consist of a typical continental crust assemblage of high-grade metamorphic rocks, such as ortho- and paragneisses, micaschists, amphibolites, and marbles (Mioč & Žnidarčič, 1977; Janák et al., 2009). These rocks form a strongly foliated matrix around elongated lenses and boudins of eclogite and ultramafic rocks, including the SBUC (Kirst et al., 2010). Abundant eclogites record peak pressures from 2.4 to 3.2 GPa (Janák et al., 2004; Sassi et al., 2004; Vrabec, 2004, 2007), based on garnet−phengite−clinopyroxene−kyanite−quartz thermobarometry, with the highest values in the southeast near the SBUC (Janák et al., 2004). Garnet peridotites within the SBUC
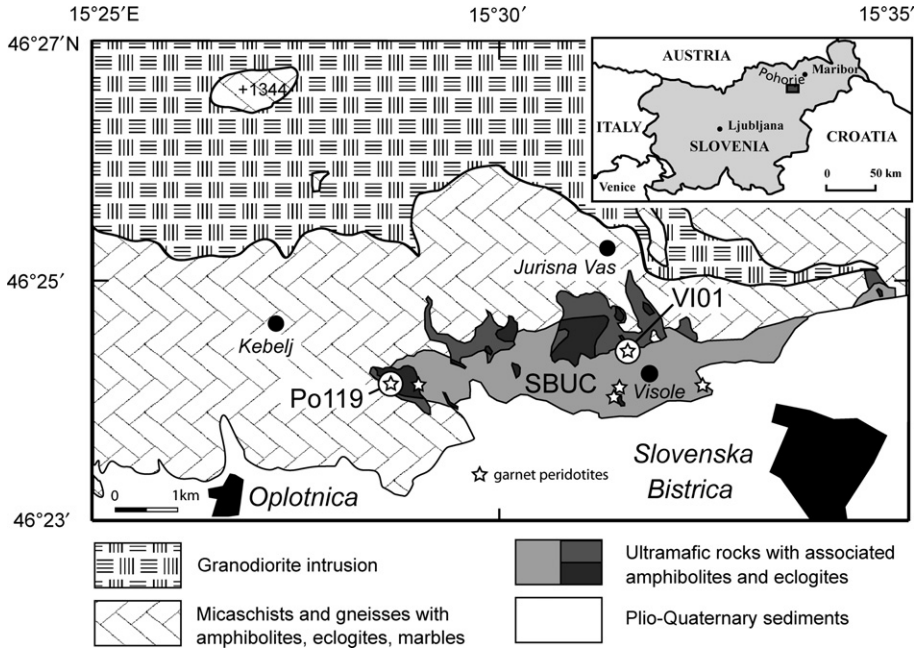
Figure 13.1 Simplified geological map of the southwest corner of the Pohorje Mountains (modified from Mioč & Žnidarčič, 1977 and Kirst et al., 2010) showing the location of the SBUC with sampling localities of garnet peridotites (Po119, VI01). Inset shows location of Slovenia and Pohorje Mountains; gray (red in the web version) rectangle indicates geological map area.

from the same localities as the ones from this study record peak pressures of up to 4 GPa based on garnet−olivine Mg−Fe exchange thermometry and Al-in-opx barometry (Janák et al., 2006). The serpentinized harzburgites from the SBUC have no recorded UHP conditions due to their simple mineralogy, which is insensitive to pressure changes, but the presence of garnet peridotites that have preserved a UHP signature points to a UHP stage (∼4 GPa) for the entire SBUC (De Hoog et al., 2009).

The Pohorje region is part of the Lower Central Austroalpine basement (Janák et al., 2004), which includes the Saualpe and Koralpe regions in Southern Austria. This unit is equivalent to the Koralpe-Wölz high-pressure nappe system of the Upper Austroalpine following Schmid et al. (2004). The region has a complicated tectonic history, which was reconstructed by Schmid et al. (2004) and is summarized here. The current Austroalpine nappes of the Eastern Alps were part of a continental block called Apulia that was bordered to the east by the Meliata ocean, the westward extension of the Neotethys and Vardar oceans (Schmid et al., 2004). The Meliata ocean opened in the Middle Triassic, and oceanic crust was formed during the Late Middle and Upper Triassic. It was subsequently subducted southeastward

during the Jurassic and was closed in the Middle Jurassic in the Western Carpathians (Maluski et al., 1993; Faryad & Henjes-Kunst, 1997). At the same time (Middle Jurassic) rifting in the north in response to the opening of the Atlantic ocean resulted in opening of the Piedmont-Liguria ocean (Frisch, 1979).

Thoni and Jagoutz (1993) suggested that the Cretaceous Austroalpine eclogites represent the westward prolongation of the Meliata (Tethys) oceanic suture into the Alps, and that this suture extended still farther west between the Southern Alps and the Austroalpine. An alternative view was presented by Janák et al. (2004), who suggested that continued convergence within Apulia during the Cretaceous was accommodated northwestward of the Meliata suture by intracontinental subduction, probably along the location of a failed Permian rift, resulting in thrusting and nappe stacking onto the northern part of the Apulian continental block The subducted crust underwent high- to UHP metamorphism, which is still preserved in Eo-Alpine eclogites. Slab extraction resulted in partial exhumation of the subducted crust (Janák et al., 2004, 2006).

The timing of HP and UHP metamorphism in the Pohorje nappe is Cretaceous, as shown by U−Pb zircon ages from the gneisses of 92.0 ± 0.5 Ma (Janák et al., 2009), a garnet Sm−Nd age (93−87 Ma) obtained from the gneisses and micaschists (Thöni, 2002), and by ~ 91 Ma garnet Sm−Nd and zircon U−Pb ages of eclogites (Miller et al., 2005). These ages are similar to those of Koralpe and Saualpe eclogite-facies metamorphism (Thöni & Jagoutz, 1992; Thöni & Miller, 1996; Miller & Thöni, 1997; Thöni, 2002), which suggests that the Koralpe−Saualpe terrane and the Pohorje massif are part of the same subducted continental crust (Janák et al., 2004, 2009). The main exhumation of the Pohorje nappe to mid-crustal levels most probably occurred during the Upper Cretaceous, but final exhumation to the surface did not occur until the Early to Middle Miocene (Fodor et al., 2002, 2003), whereas the Koralpe rocks were already exhumed during the Upper Cretaceous (Schuster et al., 2004). An earlier phase of long-lived crustal extension or rifting accompanied by HT−LP metamorphism and mafic magmatism is thought to have occurred in Permian−Triassic times (Thöni, 2002; Schuster & Stüwe, 2008).

13.2   Samples

Garnet peridotites were sampled at two locations in the SBUC (Figure 13.1), which have previously been described by Janák et al. (2006) and are listed in Table 13.1. The first location is near the village of Visole (46.41°N, 15.52°E). Sample VI01/04 is a small boulder of partially serpentinized garnet harzburgite in which the UHP metamorphic assemblage of garnet, olivine, Al-poor orthopyroxene, Al-poor clinopyroxene, and Cr-spinel is variably replaced by amphibole (pargasite), Al-rich orthopyroxene, and Al-spinel (see Janák et al., 2006 and De Hoog et al., 2009 for detailed descriptions). The second location is a larger body of $\sim 400 \times 200$ m near the farm Prihovca (46.40°N, 15.48°E). Samples with number prefix 119 are mostly garnet lherzolites that appear homogeneous without any layering, fabric, or

Table 13.1 Sample List and Mineral Contents

Sample[a]	Type[b]	Ol Fo	Opx exsolved	Cpx exsolved	Cr-Sp[c] low-Ti	Cr-Sp high-Ti	Ilm	Ap[d]
VI01/04	Gt hrz	88.6			x			
119-3	Gt lhz	88.5		Ti-rich	x	x	x	x
119-4	Gt lhz	87.7		Ti-rich	x	x	x	x
119-5	Gt lhz	86.9		Ti-poor	x			
119-5N[e]	Gt lhz	89.7		Ti-poor	x			
119-6	Gt lhz	87.6		Ti-rich	x	x	x	
119-10	Gt lhz	87.4		Ti-poor	x			
119-17	Gt lhz	89.5	x	Both	x	x	x	Incl
119-19	Gt opx	83.0	x		x		x	x
119-21	Gt lhz	90.1		Ti-poor	x			

[a]All samples contain metamorphic amphibole, pyroxene, and garnet. Samples 119-18, 119-20, and 119-22 were analyzed for whole-rock composition only.
[b]Gt hrz, garnet harzburgites (<5% Cpx); Gt lhz, garnet lherzolite; Gt opx, garnet orthopyroxenite.
[c]Low-Ti Cr-spinel defined as Cr-spinel with <0.45 wt% TiO_2.
[d]Incl, observed as inclusion only.
[e]Second offcut from same hand piece.

preferred orientation. They are considerably less serpentinized than surrounding mantle rocks and contain abundant fresh olivine, exsolved clinopyroxene, garnet, and amphibole (Figures 13.2 and 13.3; see also Janák et al., 2006). One sample contains exsolved orthopyroxene. Common accessory minerals are Cr-spinel, ilmenite, and sulfides, whereas apatite is observed in a few samples only (Table 13.1). A sample of garnet orthopyroxenite (119-19) within the peridotites is also included in this study.

The complex polymetamorphic mineral assemblage of the samples hampers identification of the primary mineral assemblage and its origin. Based on microtextural evidence, Janák et al. (2006) recognized a first stage of crystallization that includes olivine, ortho- and clinopyroxene with exsolutions (hereafter called "exsolved pyroxenes"), and Cr-spinel. These minerals are variably replaced by, overgrown by, or form inclusions in later-stage metamorphic minerals, such as amphibole, serpentine, garnet, homogeneous (unexsolved) clinopyroxene, orthopyroxene, and Al-spinel. In this study we will designate the later-stage metamorphic minerals as "metamorphic," whereas the origin of the minerals from the first stage of crystallization remains open until the Section 13.6, where we will demonstrate their dominantly igneous origin.

13.3 Analytical Techniques

Whole-rock chemical analyses of 12 samples were performed on ground powders prepared from hand pieces by crushing, grinding, and milling in an iron jaw crusher
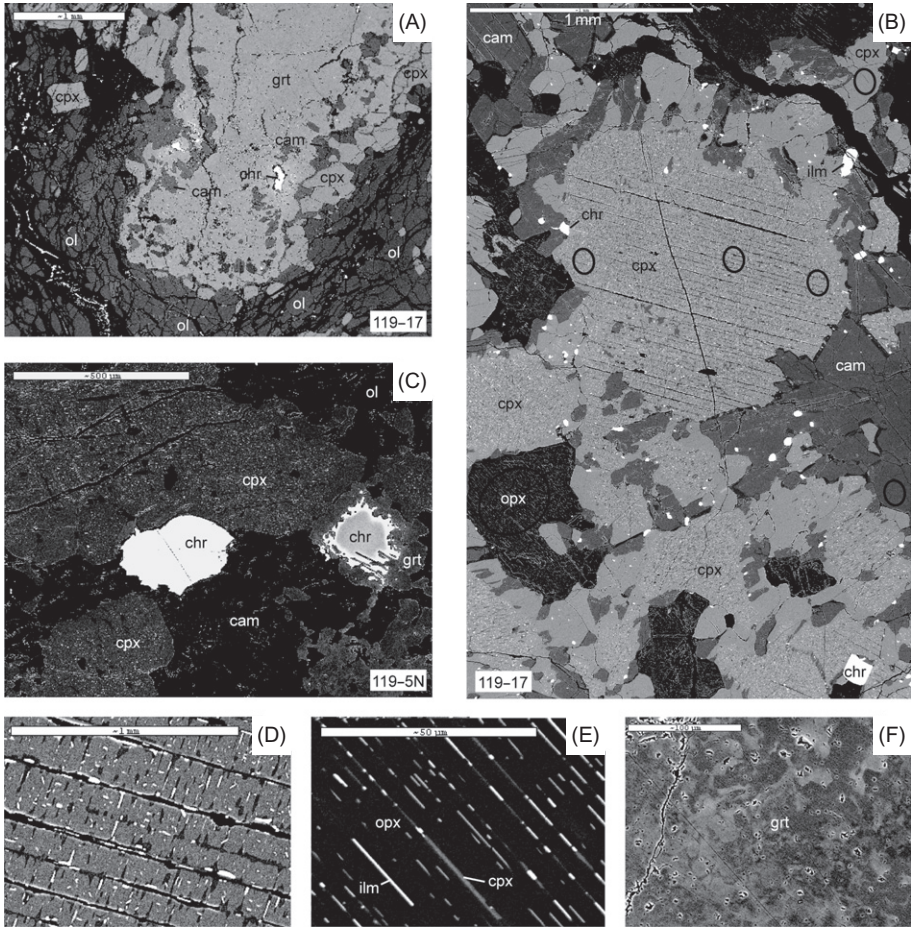
Figure 13.2 Backscatter images of thin sections. (A) Porphyroblastic garnet set in a dominantly olivine matrix. Garnet contains chromite inclusions and is partially replaced by amphibole. Olivine is partially serpentinized. (B) Exsolved clinopyroxene and orthopyroxene of magmatic origin. Clinopyroxene contains exsolutions of orthopyroxene, chromite, and ilmenite as well as amphibole (see photograph D). Orthopyroxene contains exsolutions of clinopyroxene and ilmenite (see photograph E). Metamorphic clinopyroxene is fine grained and has no exsolutions. Black ellipses indicate positions of laser-ablation ICP-MS spots. (C) Ti-rich chromite (Cr# 45, bright white) and Ti-poor chromite (Cr# 15, light gray). Ti-poor chromite has a corona of metamorphic garnet whereas Ti-rich chromite is untouched. (D) Detail of exsolved clinopyroxene in photo B. (E) Detail of exsolved orthopyroxene in photo B. (F) Example of patchy garnet surface. Light areas are more Ca-rich than darker areas but have approximately similar Mg#. Mineral abbreviations after Whitney and Evans (2010).
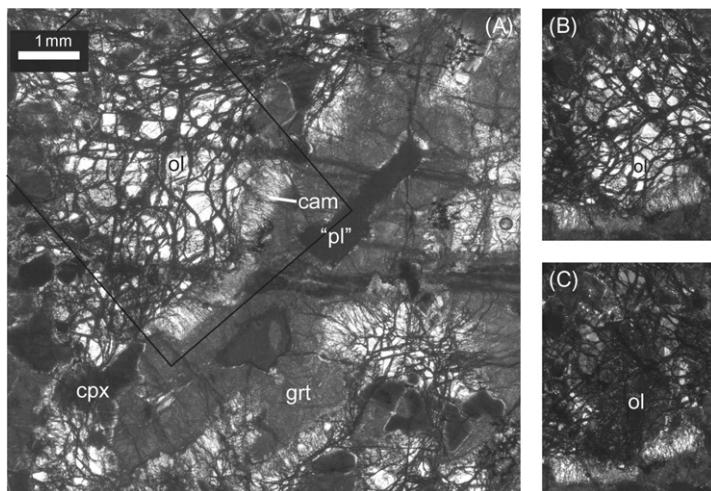
Figure 13.3 (A) Transmitted light photograph of sample 119-5 showing relict cumulate texture. We interpret the large gray lath-shaped crystal in the center as former plagioclase, partially converted to garnet (grt). The dark gray material in the core marked "pl" still preserves geochemical characteristics of plagioclase (2 wt% Na_2O, typical plagioclase REE pattern with positive Eu anomaly). A thin rim of amphibole (cam) has grown around the crystal where it is in contact with olivine. Large patches of fractured olivine (ol) are the remains of large single crystals as indicated by simultaneous extinction of neighboring grains (see photographs B and C). Also note abundant exsolved clinopyroxenes (cpx) with anhedral shapes indicative of their growth as interstitial grains. (B) Microphotograph under crossed polars showing the large olivine patch on the left side in photograph A, rotated about 40° clockwise. (C) Same area as B rotated to simultaneous extinction of olivine grains.

and agate mills and mortars. The major elements Si, Al, Mg, Fe, Cr, and Ca were determined by XRF after fusion with lithium metaborate (Geolab, Faculty of Geosciences, Utrecht University, The Netherlands). LOI was determined by heating to 1000°C after drying at 150°C.

Remaining major elements and minor and trace elements were analyzed at the Earth Science Centre (GVC) at the University of Gothenburg, Sweden, by ICP-MS following digestion of rock powders in a hot $HF-HNO_3$ mixture and analyzed by solution ICP-MS (Agilent 7500) after drying and redissolution in dilute HNO_3 with a final dilution factor of ~3800. Accuracy of the analyses was monitored on international rock standards UB-N (serpentinite), NIM-P (pyroxenites), and NIM-D (dunite); our values are generally within 10% of the recommended values. Precision of duplicate analyses is better than 5% for all elements except Nb, Th, and U (10−30%), partially due to the low levels of these elements.

Platinum-group elements (PGEs) were determined for 1.5−2 g samples by a fire assay NiS preconcentration-isotope dilution technique at the University of Ottawa,

Canada. NiS beads were dissolved in 6N HCl, after which the insoluble material in the beads (PGE) was dissolved in concentrated HNO_3 and measured by ICP-MS (HP 4500).

Mineral compositions were measured by SEM-EDS (GVC, Sweden, and Oxford, UK) following procedures described in De Hoog et al. (2010) and by electron microprobe (CAMECA SX-100) at the Dionýz Štúr Institute of Geology in Bratislava and a similar setup at the School of GeoSciences at The University of Edinburgh. Analytical conditions used in Bratislava were 15 kV accelerating voltage and 20 nA beam current, with peak counting time of 20 s and beam diameter of 2−10 μm. Raw counts were corrected using a PAP routine. Mineral standards (Si, Ca: wollastonite; Na: albite; K: orthoclase; Fe: fayalite; Mn: rhodonite), pure element oxides (TiO_2, Al_2O_3, Cr_2O_3, MgO), and metals (Ni) were used for calibration. Analytical conditions in Edinburgh were 15 kV accelerating voltage and 20 nA (major elements) and 200 nA (minor elements) beam current, with peak counting time of 20−60 s and beam diameter of 2−10 μm, except for exsolved pyroxenes, which were measured using a defocused beam of 50 μm.

Trace-element concentrations of minerals from eight samples were determined *in situ* by laser-ablation ICP-MS using a Cetac LSX-200 266 nm Nd-YAG laser system attached to a HP (now Agilent) 4500 quadrupole ICP-MS at Institute for Earth Sciences (GVC) at the University of Gothenburg. Additional analyses were done at the University of Oxford in the Department of Earth Sciences using a custom-built New Wave 193 nm ArF Excimer laser system attached to a Thermo-Finnegan Element2 magnetic sector ICP-MS in low-resolution mode. Ablation took place in He, and NIST SRM-612 was used for calibration with preferred values from Pearce et al. (1997).

Spots for laser analysis were selected after careful binocular microscopic examination of the samples to avoid cracks and inclusions in the minerals. The laser spot size was 100−200 μm, and repetition rate was 5 Hz. Each analysis consisted of 60 s measurement of gas blank and 60 s ablation. CaO contents known from EMPA were used for internal standardization. Data reduction was performed offline using in-house developed software (LaserCalc). Detection limits were 0.1 ppm for most elements, except Al, K, and Cr, 1 ppm; Na, P, and Ca, 5 ppm; and 2−10 ppb for Zr, Y, and Nb.

13.4   Whole-Rock Chemistry

13.4.1   Major and Minor Elements

The investigated rocks have high-bulk rock MgO contents (Table 13.2; 28−36 wt% on a volatile-free basis; Mg# ranges from 0.84 to 0.89 assuming FeO = 0.9 $Fe_2O_3^T$) and are also rich in Al_2O_3 (7.3−10.4 wt%) and CaO (2.6−7.5 wt%), whereas Na_2O (0.2−0.8 wt%) and TiO_2 (0.03−0.2 wt%) contents are low. The rocks contain ∼0.2 wt% Cr_2O_3 and 0.14−0.24 wt% NiO. CaO, Na_2O, and Al_2O_3 show negative

Table 13.2 Major and Trace-Element Concentrations of Pohorje Peridotites

Sample	VI01/04[c]		119-3	119-4	119-5	119-6	119-10	119-17	119-18	119-19	119-20	119-21	119-22
wt%[a]													
SiO_2	37.73		42.22	42.28	43.56	41.62	42.46	42.67	43.08	47.23	41.72	41.29	39.70
TiO_2*	0.027	0.025	0.18	0.18	0.08	0.11	0.07	0.17	0.13	0.53	0.07	0.10	0.06
Al_2O_3	7.02		7.40	8.18	8.87	10.07	9.03	9.39	8.30	9.12	8.13	8.59	6.86
Cr_2O_3*	0.25	0.26	0.21	0.22	0.20	0.25	0.15	0.23	0.26	0.13	0.16	0.21	0.25
$Fe_2O_3^T$	8.48		10.57	10.01	9.39	11.17	9.76	9.71	9.06	11.49	9.51	9.29	11.35
MnO	0.12		0.14	0.14	0.15	0.16	0.14	0.15	0.13	0.18	0.14	0.14	0.17
MgO	30.97		31.13	30.10	29.10	26.99	29.02	28.84	27.63	22.06	30.38	29.43	31.14
CaO	2.25		5.66	6.16	6.63	5.81	6.30	5.96	7.22	7.06	5.61	5.83	3.99
Na_2O	0.17		0.61	0.75	0.47	0.78	0.44	0.61	0.66	0.49	0.44	0.42	0.29
K_2O*	0.03	0.02	0.01	0.02	0.01	0.09	0.01	0.02	0.01	0.05	0.01	0.01	0.02
P_2O_5*	0.004	0.004	0.015	0.017	0.005	0.010	0.005	0.020	0.008	0.022	0.008	0.010	0.005
LOI	10.58		2.81	2.62	1.41	1.28	1.27	2.65	0.84	0.37	2.07	2.55	6.40
Ol [b]	54.1	–	59.9	59.0	49.9	55.7	52.8	52.5	48.7	18.6	56.7	55.0	62.5
Px	25.4	–	13.9	11.9	20.8	9.4	17.4	15.6	22.1	49.6	15.6	15.6	13.4
Pl	14.8	–	23.3	26.1	26.8	32.2	27.4	29.1	26.5	27.7	25.2	26.6	21.5
ppm													
Li	25.8	26.8	4.6	5.6	2.4	6.2	2.2	15.6	4.3	4.4	6.5	3.9	2.1
Sc	2.9	3.6	2.9	5.1	6.7	3.4	4.0	2.2	4.2	21.5	1.7	10.0	6.2
V	21	21	61	63	59	73	47	65	94	150	50	59	51
Co	96	97	104	100	81	102	84	104	83	73	106	109	123
Ni	1597	1696	1126	1095	1113	1020	1062	1088	1009	533	1209	1137	1259
Cu	23	13	46	40	58	19	56	84	55	93	103	86	66
Zn	41	78	60	56	30	64	27	50	33	50	45	45	69
Rb	1.07	0.40	0.40	0.45	0.32	1.44	0.15	1.06	0.48	1.88	0.49	0.26	0.22
Sr	16.6	15.4	47.3	58.5	36.4	40.7	42.1	52.5	36.8	34.0	44.0	77.4	19.9
Y	0.58	0.33	5.4	5.0	3.1	3.5	2.0	2.8	3.1	16.3	1.4	1.8	1.2
Zr	0.57	0.71	7.8	7.1	1.9	6.5	1.6	5.2	3.2	7.2	1.3	2.7	1.0
Ba	44.8	9.4	1.4	2.0	5.5	14.6	0.4	12.8	7.8	34.5	6.4	5.5	5.3

Table 13.2 (Continued)

Sample	VI01/04[c]		119-3	119-4	119-5	119-6	119-10	119-17	119-18	119-19	119-20	119-21	119-22
ppb													
Nb	160	95	120	138	76	126	72	83	35	544	16	46	21
Cs	587	373	131	107	61	215	57	358	83	269	89	154	64
La	203	96	252	302	657	273	274	350	373	306	93	204	145
Ce	519	322	960	1176	308	726	263	796	371	644	205	491	300
Pr	69	47	188	226	157	172	66	160	96	153	36	74	50
Nd	346	257	1223	1459	750	1218	389	880	555	1026	243	395	283
Sm	79	65	467	502	236	501	136	295	223	572	95	143	93
Eu	68	50	182	209	138	230	124	163	135	258	95	109	83
Gd	102	78	697	683	365	664	234	412	391	1221	170	238	138
Tb	15	10	125	124	65	107	47	76	77	296	31	42	25
Dy	104	62	883	840	449	635	309	472	511	2416	228	310	201
Ho	19	10	195	177	98	127	70	100	109	593	48	61	42
Er	59	31	565	518	295	336	212	283	329	1871	145	193	134
Tm	10	6	81	72	40	47	31	48	53	302	19	31	19
Yb	70	42	537	478	264	290	205	292	296	2052	145	203	140
Lu	12	8	80	76	42	47	33	53	53	307	24	33	23
Hf	33	44	338	306	118	292	122	168	124	279	50	52	40
Pb	532	499	336	344	332	1013	170	908	546	6264	527	1027	778
Th	30	9	9	5	3	4	6	5	<4	22	<4	6	<4
U	5	5	6	<4	<4	<4	4	8	<4	8	<4	15	8
Os	0.61	2.11	–	0.04	0.05	–	0.07	0.07	0.07	0.06	0.02	0.04	0.14
Ir	1.33	2.58	–	0.17	0.14	–	0.16	0.10	0.10	0.09	0.13	0.10	0.18
Ru	1.54	3.78	–	0.39	0.38	–	0.51	0.20	0.24	0.12	0.23	0.16	0.34
Rh	0.36	0.44	–	0.08	0.13	–	0.09	0.07	0.07	0.06	0.14	0.07	0.08
Pt	2.80	2.40	–	0.96	0.59	–	0.74	0.71	0.58	0.50	1.10	0.67	1.35
Pd	2.43	2.17	–	1.32	1.30	–	0.87	1.37	1.58	0.89	1.39	1.21	2.11

[a]Major elements by XRF except for oxides indicated by * by ICP-MS; all Fe as Fe_2O_3.
[b]Weight modes of Ol, Px, and Pl from CIPW norm calculation assuming FeO = 0.9 $Fe_2O_3^T$.
[c]Separate digestions of two parts of one hand piece.
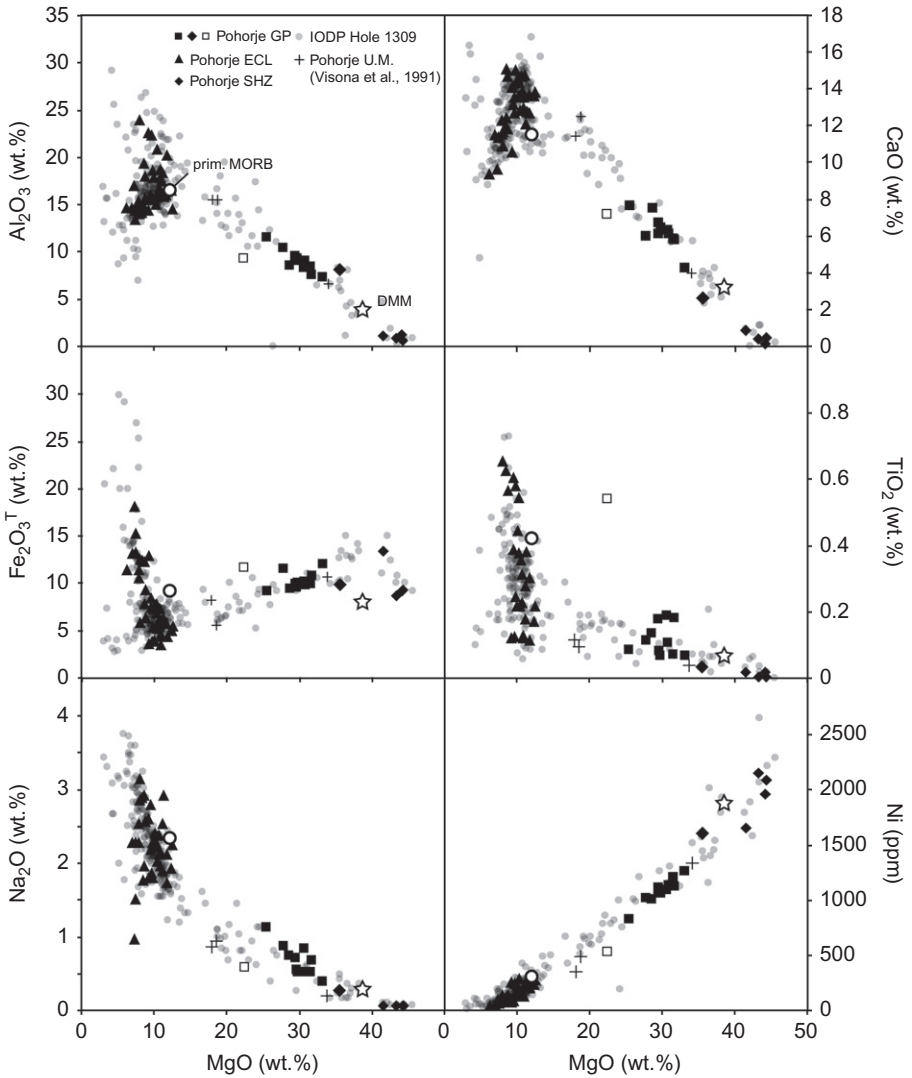
Figure 13.4 Selected whole-rock major and minor element compositions of Pohorje mafic and ultramafic rocks plotted against whole-rock MgO contents. A compilation of rock analyses from IOPD Site U1309 (an oceanic core complex on the MAR; Godard et al., 2009) is plotted for comparison, as well as model compositions of primary MORB (Herzberg & O'Hara, 2002) and depleted MORB mantle (DMM), the source of MORB (Workman & Hart, 2005). Pohorje data: SHZ, serpentinized harzburgites (De Hoog et al., 2009); ECL, eclogites (Vrabec, 2007); GP, garnet peridotites and pyroxenite (this study). Crosses: SBUC troctolite, garnet peridotite, and pyroxenite from Visona et al. (1991).

correlations with MgO, whereas Ni shows a strongly positive correlation (Figure 13.4). $Fe_2O_3^T$ and TiO_2 are more scattered, but Na_2O and P_2O_5 show good correlations with TiO_2. The major elements contents fall in between the compositions of Pohorje eclogites and serpentinites (Figure 13.4) and are comparable to those of olivine-rich troctolites from the Mid-Atlantic Ridge (MAR; Godard et al., 2009). The garnet orthopyroxenite sample (119-19) has considerably higher TiO_2 (0.54 wt%) and lower MgO (22.4 wt%) than the other samples.

13.4.2 Trace Elements

Bulk-rock incompatible trace elements are generally low (Table 13.2; e.g., Zr 0.7−8 ppm, Nb <0.2 ppm, Y <6 ppm), except for garnet orthopyroxenite 119-19 (Zr 7.3 ppm, Nb 0.5 ppm, Y 17 ppm), and show weak negative correlations with MgO (Figure 13.5). Alkali and alkaline earth elements are generally less depleted (Sr 20−60 ppm, Ba 1−60 ppm, Li 2−20 ppm). This is particularly obvious for sample VI01/04, which is otherwise the most depleted but has the highest Rb, Sr, and Ba contents. As in the case of major elements, most trace-element contents fall in between those of eclogites and serpentinized harzburgites from Pohorje (De Hoog et al., 2009) and are comparable to those of ultramafic cumulates from the MAR (Godard et al., 2009), apart from their elevated Ba and Cs contents (Figure 13.5). Positive correlations exist between TiO_2 and several trace elements (V, Sr, Y, Zr, REE).

Rare earth element patterns are characterized by relatively flat and parallel patterns (Figure 13.6). Samples with high TiO_2 have no small positive Eu anomalies, relatively high total REE contents (1−3 times chondrite), and LREE depletions, although La contents are variable. Samples with low TiO_2 have low total REE contents (0.4−1.5 times chondrite), strong positive Eu anomalies, and variable LREE contents. One sample, 119-5, has a strong negative Ce-anomaly. Sample VI01/04 is the only sample with a LREE-enriched pattern, comparable to serpentinized harzburgites from Pohorje (De Hoog et al., 2009). Sample 119-19 (garnet orthopyroxenite) shows a strongly LREE-depleted pattern with rather high HREE (10 times chondrite).

Incompatible elements, including REE, are strongly depleted relative to primitive mantle and N-MORB (Figure 13.7), but Sr shows a strong positive anomaly for all samples. Rubidium and Ba are enriched relative to other elements as well, whereas U is enriched in some samples and depleted in others. A small negative anomaly for Zr is observed, probably related to low partitioning of Zr into Cpx and plagioclase, the main trace element−bearing phases in the protolith (see Section 13.5.2). Niobium is rather variable but not depleted relative to Th.

PGE concentrations are very low (<0.5 ppb Os, Ir, Ru, and Rh) apart from sample VI01/04, which has 0.4−1.5 ppb Os, Ir, Ru, and Rh. $(Pd/Ir)_N$ ratios vary from 4.6 to 10.9 for samples from locality 119 and 0.7 to 1.5 for two aliquots of sample VI01/04.
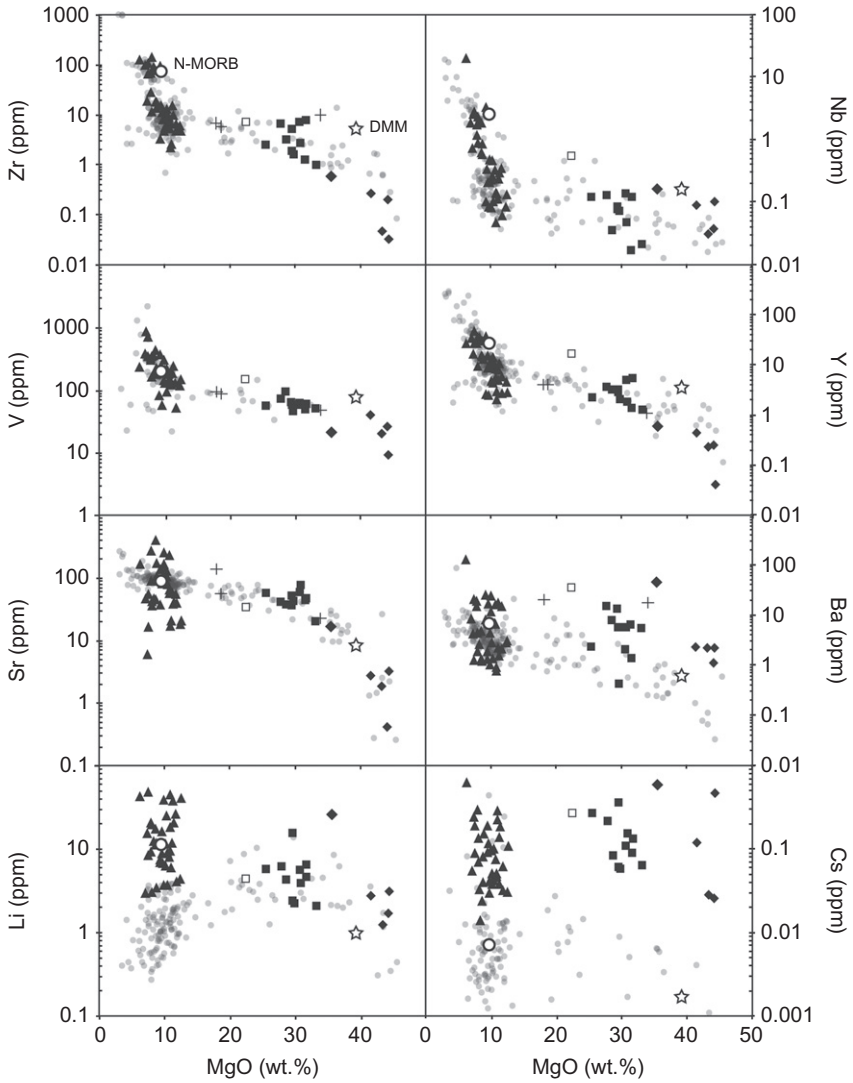
Figure 13.5 Selected whole-rock trace-element compositions of Pohorje mafic and ultramafic rocks plotted against MgO contents. Analyses of rocks from IOPD Site U1309 is plotted for comparison (Godard et al., 2009), as well as model compositions of N-MORB (V: Shervais, 1982; other elements: Sun & Mcdonough, 1989) and DMM (Workman & Hart, 2005); Cs, Li, and V are calculated from primitive mantle (PM) values in McDonough and Sun (1995), and estimated from DMM/PM ratios. Pohorje data: symbols as in Figure 13.4.
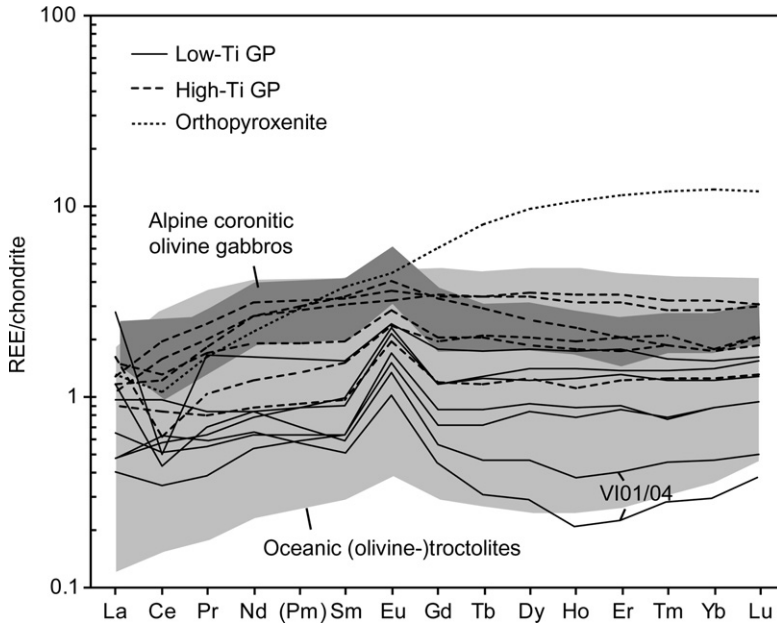
Figure 13.6 Whole-rock REE compositions of Pohorje peridotites relative to CI chondrite (McDonough & Sun, 1995). Compositions of coronitic olivine gabbros from the Ötztal complex (Miller & Thöni, 1995) and a compilation of olivine-rich cumulates from IOPD Site U1309 (an oceanic core complex on the MAR; Godard et al., 2009) are shown for comparison.

13.5　Mineral Chemistry

13.5.1　Major Elements

13.5.1.1　Olivine

Olivine occurs as euhedral to subhedral grains that form large patches in the matrix of the rocks (Figure 13.3). Many of these are highly fractured remnants of former larger grains, as indicated by simultaneous extinction of clusters of olivine grains under crossed polars (Figure 13.3), but fine-grained recrystallized olivine has been observed as well. It is occasionally found as inclusions in garnet. Forsterite contents of olivine fall mostly between 86.5 and 90.3, with a few grains down to 82 and up to 91.0 (Table 13.3). They show little zoning, except for a few grains in sample 119-6. NiO contents show a very narrow range from 0.23 to 0.27 wt% except for VI01/04 (0.28−0.35 wt%) and 119-5N (0.24−0.32 wt%), and show little correlation with Fo content. Most samples have very uniform compositions throughout the thin section, with Fo contents within 1 unit and NiO variation no more than 0.03 wt%. MnO contents are more variable (0.03−0.18 wt%) and show
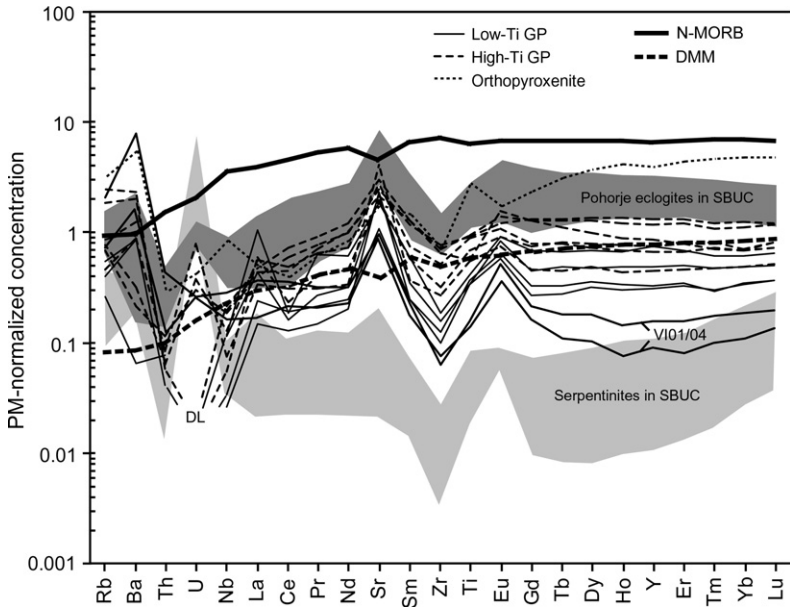
Figure 13.7 Whole-rock trace-element compositions of Pohorje peridotites normalized to primitive mantle (McDonough & Sun, 1995). The dark- and light-gray fields comprise the compositions of Pohorje eclogites within the SBUC (Vrabec, 2007) and SBUC-serpentinized harzburgites (De Hoog et al., 2009), respectively. Compositions of N-MORB (Sun & Mcdonough, 1989) and DMM (Workman & Hart, 2005) are indicated for comparison.

a well-defined negative correlation with Fo content, apart from sample VI01/04, which has relatively high MnO relative to the other samples (0.17 wt% MnO at Fo88.3 instead of 0.08 wt%). Other elements (CaO, Al_2O_3, Cr_2O_3) are all less than 0.01 wt% in all the samples. Rare olivine in sample 119-19 (garnet orthopyroxenite) has Fo83 with relatively low MnO contents (0.15 wt%).

13.5.1.2 Orthopyroxene

Orthopyroxene occurs mostly as small grains in the sample matrix and as inclusions and exsolution lamellae in clinopyroxene, but several large exsolved orthopyroxenes are observed in samples 119-17 and 119-19 (Figure 13.2B). Only in sample 119-19 (garnet orthopyroxenite) is Opx a major constituent and coarse grained. Matrix Opx is magnesian (Mg# 0.88−0.91, but variable and lower in 119-19: Mg# 0.81−0.87; Table 13.3). CaO is low (0.05−0.29 wt%), as is TiO_2 (<0.1 wt%) and Cr_2O_3 (<0.12 wt%), whereas Al_2O_3 is rather variable (0.4−1.8 wt%). Inclusions in clinopyroxene have similar compositions.

Large exsolved orthopyroxenes with exsolution lamellae of clinopyroxene and smaller exsolutions of ilmenite and Cr-spinel are observed in samples 119-17 and

Mineral	Cpx		Opx	Cam		Grt			Cr				Ol				Ilm		Ap
Sample	119-19	119-5N	119-19	119-17	119-5N	119-5N	119-19	119-4	119-21	119-17	VI01/04	119-5	119-21	119-19	VI01/04	119-10	119-19	119-17	119-3
Lab	Br	Ed	Br	Ed	Ed	Ed	Br	Ed	Oxf	Oxf	Oxf	Ed	Ed	Br	Ed	Ed	Oxf	Oxf	Oxf
Stage[a]	II	III	II	III	III	II	II	II	I–III	I–III	I–III	I–III	I–III	I–III	I–III	I–III	I–III	I–III	I–III
SiO_2	55.14	54.84	56.50	45.38	45.31	41.65	41.41	41.37	0.14	0.09	0.12	0.07	40.90	40.13	40.84	40.22	0.10	0.08	
P_2O_5																			42.51
TiO_2	0.05	0.07	0.04	0.36	0.43	0.03	0.06	0.03	0.07	1.25	0.12	0.05	<0.01	0.06	<0.01	<0.01	54.77	54.10	
Al_2O_3	1.27	1.06	0.87	12.90	13.63	23.81	22.14	23.29	27.98	16.05	25.76	47.75	<0.01	0.01	<0.01	<0.01	0.18	0.17	
V_2O_5									0.07	0.41	0.10								
Cr_2O_3	0.10	0.09	0.03	1.11	0.42	0.05	0.09	0.03	36.74	35.63	40.63	19.40	<0.01	0.01	<0.01	<0.01	0.31	0.17	
Fe_2O_3[b]									4.19	13.50	1.24	1.20							
FeO	3.37	1.66	9.00	4.05	3.30	10.57	14.66	13.56	19.74	26.01	19.74	15.51	9.80	16.14	11.16	12.20	44.25	43.80	0.36
MnO	0.02	0.01	0.11	0.04	0.01	0.29	0.49	0.50	0.20	0.23	0.34	0.12	0.05	0.15	0.16	0.10	0.45	2.68	
NiO				0.07	0.10				0.11	0.21	0.08	0.16	0.27		0.31	0.25			
MgO	17.23	17.54	33.05	18.76	19.37	17.43	15.81	16.14	10.81	6.14	10.22	15.57	49.71	44.17	48.69	47.63	3.09	0.70	0.41
CaO	23.89	24.36	0.14	12.22	11.92	6.81	4.75	5.82	0.03	0.01		0.01	<0.01	0.05	<0.01	<0.01		0.02	55.42
ZnO									0.31	0.47	0.35	0.09							
Na_2O	0.56	0.50		2.45	2.93	<0.01		0.01										0.01	
K_2O		<0.01		0.04	0.02	<0.01		<0.01											0.04
Cl																			2.18
Total	101.63	100.12	99.74	99.49	99.55	100.64	99.41	100.74	100.41	100.00	98.70	99.92	100.72	100.72	101.16	100.40	103.16	101.73	101.68

O	6	6	6	23	23	12	12	12	4	4	4	4	4	4	4	4	6	6	25
Si	1.977	1.984	1.975	6.429	6.386	2.977	3.040	2.990	0.004	0.003	0.004	0.002	0.995	1.004	0.996	0.994	0.005	0.004	0.000
P	0.000	0.000	0.000	0.000	0.000	0.000	0.000	0.000	0.000	0.000	0.000	0.000	0.000	0.000	0.000	0.000	0.000	0.000	5.986
Ti	0.001	0.002	0.001	0.038	0.045	0.002	0.003	0.002	0.002	0.031	0.003	0.001	0.000	0.000	0.000	0.000	1.973	2.001	0.000
Al	0.054	0.045	0.036	2.154	2.263	2.006	1.915	1.984	1.004	0.629	0.948	1.547	0.000	0.000	0.000	0.000	0.010	0.010	0.000
V^{5+}	0.000	0.000	0.000	0.000	0.000	0.000	0.000	0.000	0.001	0.009	0.002	0.000	0.000	0.000	0.000	0.000	0.000	0.000	0.000
Cr	0.003	0.002	0.001	0.124	0.046	0.003	0.005	0.002	0.884	0.937	1.003	0.422	0.000	0.000	0.000	0.000	0.012	0.007	0.000
Fe^{3+}	0.000	0.000	0.000	0.000	0.000	0.000	0.000	0.000	0.096	0.338	0.029	0.025	0.000	0.000	0.000	0.000	0.000	0.000	0.000
Fe^{2+}	0.101	0.050	0.263	0.480	0.389	0.632	0.900	0.819	0.502	0.724	0.516	0.357	0.199	0.338	0.228	0.252	1.772	1.801	0.051
Mn	0.001	0.000	0.003	0.005	0.002	0.017	0.030	0.031	0.005	0.006	0.009	0.003	0.001	0.003	0.003	0.002	0.018	0.112	0.000
Ni	0.000	0.000	0.000	0.007	0.011	0.000	0.000	0.000	0.003	0.006	0.002	0.003	0.005	0.000	0.006	0.005	0.000	0.000	0.000
Zn	0.000	0.000	0.000	0.000	0.000	0.000	0.000	0.000	0.007	0.012	0.008	0.002	0.000	0.000	0.000	0.000	0.000	0.000	0.000
Mg	0.921	0.946	1.722	3.962	4.070	1.857	1.730	1.739	0.490	0.304	0.476	0.638	1.804	1.647	1.771	1.754	0.221	0.051	0.103
Ca	0.917	0.944	0.005	1.855	1.800	0.522	0.374	0.450	0.001	0.000	0.000	0.000	0.000	0.000	0.000	0.000	0.000	0.001	9.877
Na	0.039	0.035	0.000	0.673	0.800	0.000	0.000	0.001	0.000	0.000	0.000	0.000	0.000	0.000	0.000	0.000	0.000	0.001	0.000
K	0.000	0.000	0.000	0.007	0.004	0.000	0.000	0.000	0.000	0.000	0.000	0.000	0.000	0.000	0.000	0.000	0.002	0.000	0.008
Cl	0.000	0.000	0.000	0.000	0.000	0.000	0.000	0.000	0.000	0.000	0.000	0.000	0.000	0.000	0.000	0.000	0.000	0.000	0.614
Sum	4.013	4.008	4.006	17.734	17.816	8.017	7.997	8.017	3.000	3.000	3.000	3.000	3.005	2.992	3.004	3.006	4.012	3.988	18.024
Mg#[c]	0.90	0.95	0.87	0.89	0.91	0.75	0.66	0.68	0.49	0.30	0.48	0.64	0.90	0.83	0.89	0.87	0.11	0.03	0.67
Cr#[d]	0.05	0.05	0.02	0.05	0.02	0.00	0.00	0.00	0.47	0.60	0.51	0.21					0.53	0.41	

[a] I, protolith stage; II, UHP stage; III, exhumation stage; I–III, mineral present through all stages (Janák et al., 2006).
[b] Fe_2O_3 calculated from stoichiometry.
[c] Mg# = Mg/(Mg + Fe).
[d] Cr# = Cr/(Cr + Al).

Table 13.4 Averaged Major Element Compositions of Exsolved Pyroxenes

Sample	119-3	119-4	119-5	119-5N	119-10	119-17	119-17	119-17	119-21
Mineral	Cpx	Cpx	Cpx	Cpx	Cpx	Cpx	Cpx	Opx	Cpx
No. of analyses	6	6	6	7	7	4	4	5	11
SiO_2	51.75	52.09	51.20	51.63	50.02	50.68	51.03	55.36	51.17
TiO_2	0.94	0.90	0.50	0.36	0.48	0.38	1.55	0.51	0.40
Al_2O_3	2.77	2.41	3.24	2.92	3.12	3.42	2.91	1.89	3.17
Cr_2O_3	1.18	1.12	1.37	1.35	1.21	1.32	1.26	0.56	1.32
FeO*	3.55	3.35	2.66	2.70	2.80	3.33	3.75	6.95	2.81
MnO	0.05	0.04	0.08	0.03	0.09	0.05	0.04	0.08	0.06
NiO	0.03	0.02	0.03	0.03	0.02	0.03	0.03	0.04	0.03
MgO	17.49	17.28	16.14	17.97	16.49	18.56	17.72	33.05	17.58
CaO	21.28	21.97	21.75	20.62	21.80	20.15	20.98	1.78	20.88
Na_2O	0.82	0.79	1.19	0.79	1.07	0.66	0.80	0.09	0.87
K_2O	<0.01	<0.01	<0.01	<0.01	<0.01	<0.01	<0.01	<0.01	<0.01
Total	99.86	99.98	98.18	98.39	97.10	98.58	100.09	100.31	98.27
Si	1.894	1.905	1.904	1.906	1.886	1.874	1.868	1.924	1.896
Ti	0.026	0.025	0.014	0.010	0.014	0.011	0.043	0.013	0.011
Al	0.119	0.104	0.142	0.127	0.139	0.149	0.126	0.077	0.138
Cr	0.034	0.032	0.040	0.039	0.036	0.039	0.036	0.015	0.039
Fe	0.109	0.103	0.083	0.083	0.088	0.103	0.115	0.202	0.087
Mn	0.001	0.001	0.003	0.001	0.003	0.002	0.001	0.002	0.002
Ca	0.834	0.861	0.867	0.816	0.881	0.798	0.823	0.001	0.829
Mg	0.955	0.942	0.895	0.989	0.927	1.023	0.967	1.712	0.971
Ni	0.001	0.001	0.001	0.001	0.001	0.001	0.001	0.066	0.001
Na	0.058	0.056	0.086	0.057	0.079	0.047	0.057	0.006	0.062
Sum	4.032	4.030	4.034	4.029	4.052	4.046	4.037	4.020	4.036
En	50.3%	49.4%	48.5%	52.4%	48.8%	53.1%	50.7%	86.3%	51.4%
Wo	43.9%	45.1%	46.9%	43.2%	46.4%	41.4%	43.2%	3.3%	43.9%
Fs	5.8%	5.4%	4.6%	4.5%	4.8%	5.4%	6.1%	10.3%	4.7%
Mg#	89.8%	90.2%	91.5%	92.2%	91.3%	90.9%	89.4%	89.5%	91.8%

All Fe as FeO, cation formula based on 6O, En = Mg/(Mg + Ca + Fe + Mn); Wo = Ca/(Mg + Ca + Fe + Mn); Fs = Fe/(Mg + Ca + Fe + Mn); Mg# = Mg/(Mg + Fe).

119-19. In the former, integrated analyses over a 300 μm^2 area on two large grains (Table 13.4) yields high CaO (1.8 wt%), TiO_2 (0.5 wt%), and Cr_2O_3 (0.6 wt%). Exsolved Opx in 119-19 has a similar composition apart from markedly lower Cr_2O_3 contents (0.06 wt%). Metamorphic Opx in the same sample has low TiO_2 (0.03 wt%), CaO (0.13 wt%), and Na_2O (0.003 wt%).

13.5.1.3 Clinopyroxene

Clinopyroxene occurs as large anhedral crystals with exsolution lamellae of orthopyroxene and smaller exsolutions of ilmenite and Cr-spinel, as small homogenous grains in the sample matrix, and as exsolution lamellae in orthopyroxene (Figure 13.2B). They can be divided into three groups based on their composition: high-Ti exsolved Cpx (0.6−1.8 wt% TiO_2), low-Ti exsolved Cpx (0.3−0.6 wt% TiO_2), and metamorphic Cpx with no exsolutions (<0.2 TiO_2). Low-Ti Cpx was found in samples 119-5, 119-5N, 119-10, 119-17, and 119-21, whereas high-Ti Cpx is restricted to samples 119-3, 119-4, and 119-17. Only in the latter sample were both types observed together. In this sample, low-Ti and high-Ti Cpx form separate grains, bar one low-Ti Cpx which has a rim of high-Ti Cpx. Exsolved Cpx are usually rimmed by metamorphic Cpx.

Matrix clinopyroxenes and metamorphic rims surrounding exsolved Cpx are magnesian diopsides (Mg# 0.925−0.946; Table 13.3) with a narrow range of CaO contents (24.1−24.8), variable Al_2O_3 and Na_2O contents (0.5−1.4 and 0.2−1.1, respectively), and low jadeite and tschermak components (0.01−0.04). Cr_2O_3 contents are <0.3 wt% except in samples 119-3, 119-21, and 119-5N up to 0.8 wt%.

Compositions of exsolved clinopyroxenes overlap with matrix ones but extend to lower Mg# and CaO and higher Na_2O, Al_2O_3, Cr_2O_3, and TiO_2 contents. To estimate the compositions of clinopyroxenes before exsolution, several domains were analyzed with a 50 μm defocused beam. Averages of 5−8 analyses per sample indicate that original CaO contents ranged from 20.1 to 22.0 wt%, with Mg# between 89.4 and 92.2 (Table 13.4). Low-Ti Cpx has a narrow range of TiO_2 contents (0.36−0.48 wt%), whereas Ti-rich Cpx is rather variable (0.5−1.8 wt%) and has lower Mg# than Ti-poor Cpx.

The compositions of Ti-poor Cpx are virtually identical to that of Cpx from olivine-rich troctolites and gabbros from the MAR (Drouin et al., 2009). Clinopyroxene from this locality also has exsolutions of Opx, which indicates that exsolution started during igneous cooling.

13.5.1.4 Garnet

Garnet occurs as large subhedral porphyroblasts and as coronas surrounding Cr-spinel. It was also found as exsolution in clinopyroxene from sample 119-5 (Janák et al., 2006). Occasionally it has inclusions of Cr-spinel and apatite. Garnet compositions are rather variable on a small scale in many grains, giving them a patchy appearance in backscatter imaging. Pyrope content ranges from 72% to 78%, with a few grains down to 66% (Table 13.3). CaO is generally between 4.5 and

6.5, but values up to 9.6 are observed in particularly patchy garnets. Cr_2O_3 contents are generally <0.2 wt%, although several garnets in samples VI01/04B, 119-17, 119-5N, and 119-3 contain small domains with up to 1.5 wt% Cr_2O_3, often in areas where spinel inclusions are also found. TiO_2 contents are very low in all garnets (<0.06 wt%). MnO is variable (0.2−0.7, up to 1.2 in 119-19) and correlates strongly with Mg#.

13.5.1.5 Spinel

Spinel is a common phase in all samples except 119-19 and occurs as euhedral to subhedral grains in the sample matrix, as partially resorbed grains with garnet coronas (Figure 13.2C), as exsolutions in pyroxenes, and as inclusions in garnet. It shows a wide range of compositions: Mg# from 0.25 to 0.8 and Cr# from 0 to 0.6 (Table 13.3; Figure 13.8A). Spinels with Mg# higher than 0.5 have low TiO_2 contents (<0.3 wt%), whereas spinels with Mg# less than 0.4 show increasing TiO_2 up
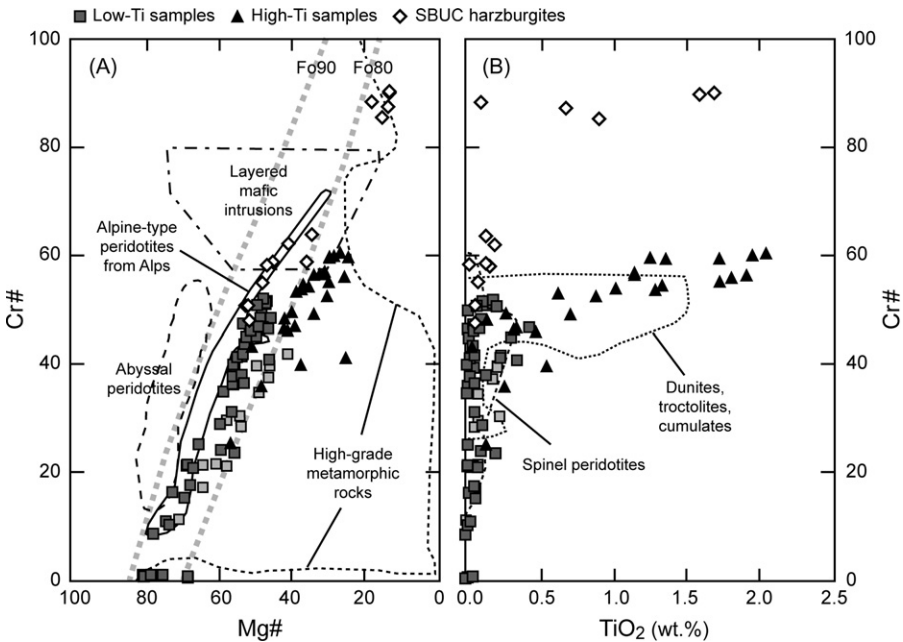
Figure 13.8 Cr-spinel compositions of Pohorje garnet peridotites with compositional fields after Dick and Bullen (1984). Compositions of Cr-spinels from harzburgites from the SBUC are indicated for comparison. (A) Mg#−Cr# diagram showing two different trends for spinels from Pohorje garnet peridotites; gray dashed lines indicate olivine compositions in equilibrium with spinel (Dick & Bullen, 1984). (B) TiO_2 (wt%)−Cr# diagram. TiO_2-rich spinels are limited to samples with high-TiO_2 Cpx (Figure 13.9) and the low-Mg# spinel trend in A.

to 2.1 wt% (Figure 13.8B). MnO contents are scattered and range from 0.1 to 0.6 wt%. ZnO contents are variable as well, being 0.4 wt% on average but up to 1.1% in some spinels.

Two parallel trends with different Mg# for given Cr# can be distinguished in a Mg#−Cr# diagram (Figure 13.8A). Cr-spinels from samples 119-21, VI01/04, 119-10, and 119-5N have Mg# 0.57 at Cr# 0.4, whereas other samples have Mg# 47. In the latter samples Ti-rich spinels coexist with TiO_2-poor spinels, whereas the spinels with high Mg# have TiO_2 contents less than 0.5 wt% (Figure 13.8B). Generally, TiO_2- and Cr_2O_3-rich spinels are euhedral, whereas others are variably replaced by garnet (Figure 13.2C). Many spinels are strongly zoned, usually becoming more Fe-, Cr-, and Ti-rich toward the rims, but the opposite also occurs. Outer rims are always the most Cr_2O_3-rich; rims touching garnets are usually also strongly enriched in Cr_2O_3. TiO_2-poor spinels are typical of spinel peridotites, whereas TiO_2-rich spinels are commonly found in dunites, plagioclase peridotites, and cumulates as a result of equilibration with TiO_2-bearing melts (Figure 13.8B).

Spinels from the high-Mg# trend fall near the field of Alpine peridotites, but Mg# for given Cr# are lower than expected based on equilibrium with olivine (Figure 13.8A), which is most likely due to reequilibration of Mg# to lower temperatures during cooling or metamorphic overprint (Barnes, 2000). Spinels from the low-Mg# trend plot even further away, which suggests they are in equilibrium with olivine with a lower Fo content. The samples have indeed lower Fo content than most others (Fo90 vs. Fo88), although sample 119-17 has high Fo but nevertheless falls in the low-Mg# spinel field.

13.5.1.6 Amphibole

Ca-amphibole is very common and replaces garnet and clinopyroxene (Figure 13.2A and C). It is mostly pargasitic. Mg# range from 0.85 to 0.91, and Cr_2O_3 varies widely from <0.1 to 2.5 wt% (Table 13.3). Low Cr_2O_3 amphiboles are mostly associated with garnet, whereas high Cr_2O_3 amphiboles are mostly associated with Cpx. TiO_2 contents are mostly between 0.25 and 0.45 wt% but are less than 0.2 wt% in sample VI01/04. Higher values up to 0.8 wt% are from amphibole inclusions in Cpx. It occurs as euhedral inclusions in some garnets, which suggests Ca-amphibole may have been part of the pre-UHP assemblage. In samples 119-6 and VI01/04, Ca-poor amphibole (gedrite) is observed in the matrix.

13.5.1.7 Other Minerals

Serpentine is present in all samples, replacing olivine and exsolved orthopyroxene, but only in sample VI01/04 serpentinization was extensive, as indicated also by its high LOI value (10.6 wt%).

Chlorite (clinochlore) is found in the matrix of samples 119-6 and VI01/04.

Plagioclase with an anorthite content around 80% was occasionally observed as the breakdown product of omphacite.

Corundum was observed as inclusions in garnet in several samples (Vrabec, 2007).

Ilmenite is common in 119-19 and also present in several other samples (119-17, 119-6, 119-3, 119-4) as subhedral grains up to 200 μm. It contains up to 6.7 wt% MgO and 2.6 wt% MnO, but <0.4 wt% Al_2O_3 and Cr_2O_3. In sample 119-19 it shows exsolutions of magnetite with high contents of Al_2O_3 (6.8 wt%), TiO_2 (4 wt%), Cr_2O_3 (16 wt%), and notably high V_2O_5 (7.7 wt%).

Sulfides with high Fe and Ni but low Cu contents are observed in the matrix of most samples.

Apatite occurs as euhedral grains in the matrix and as inclusions up to 200 μm in garnet from samples 119-3, 119-17, 119-4, and 119-19. It is rich in chlorine (0.9−3.0 wt%).

Zircon was found as a single 20-μm grain in the matrix of sample 119-3.

13.5.2 Trace Elements

13.5.2.1 Clinopyroxene

Laser-ablation analysis of exsolved pyroxenes yields an average analysis of clinopyroxene including exsolved phases (Figure 13.2B). High-Ti exsolved Cpx is characterized by high contents of TiO_2, K_2O, Sr, Ba, Zr, Nb, U, and LREE relative to low-Ti Cpx, but low contents of Sc, V, Cr, and low Mg# (Table 13.5). Other compatible elements (Mn, Co, Ni) are very similar. Metamorphic Cpx has low contents of all trace elements with the exception of Sr, La, and Pb, which are comparable to low-Ti Cpx. Of the three types, matrix Cpx has the most constant composition, whereas exsolved Cpx shows large variations and sometimes strong zoning. Significant variations between Cpx from different samples are observed for most elements. For instance, Ti-poor Cpx in sample 119-5N has high Sr but much lower Nb than Ti-poor Cpx from samples 119-17 and 119-21. Compositions of Ti-rich Cpx show considerably less variation between different samples.

Rare earth element patterns of Cpx are generally LREE and HREE depleted, but the range in HREE is much larger than LREE in both high-Ti and low-Ti Cpx (Figure 13.9A). Zoned crystals show strong decreases in HREE from core to rim but only limited simultaneous decrease in MREE−LREE. High-Ti Cpx shows negative Eu anomalies, which are the most pronounced in those parts of the grains with the highest REE contents, generally the crystal cores. Low-Ti Cpx shows only very small negative Eu anomalies in cores, whereas rims have no Eu anomalies. Metamorphic Cpx has strongly depleted HREE and no Eu anomalies.

Trace-element patterns are quite similar to those of Cpx from olivine-rich gabbros and troctolites from the MAR (Drouin et al., 2009), apart from high Sr and HREE depletions in Cpx from Pohorje garnet peridotites (Figures 13.9A and 13.10). Ti-poor Cpx patterns compare well to those of MAR Cpx cores, whereas Ti-rich patterns are more similar to MAR interstitial Cpx and Ti-rich rims (Figure 13.10).

<div align="center">

Table 13.5 Trace-Element Compositions of Selected Minerals

</div>

Sample	119-21	119-17	119-17	119-17	119-4	119-4	119-17	119-19	119-19	119-17	119-5N	119-19	119-5
Grain	Cpx-2	Cpx-1b	Cpx-1c	Cpx-1e	Cpx-1a	Cpx-1c	Opx-3d	Opx-1b	Opx-n	Amph-2	Gt-1	Gt-2	'Pl'
Domain	Core	Core	Rim	New [a]	Core	Rim	Core	Core	New	New	Core	Core	Core[b]
wt%													
CaO	24.0	22.5	22.5	25.0	22.0	22.0	1.7	1.8	0.10	12.5	6.0	5.0	17.0
TiO$_2$	0.46	0.56	0.52	0.07	1.88	2.38	0.59	0.36	0.03	0.45	0.02	0.02	0.04
Cr$_2$O$_3$	0.76	1.48	1.43	0.28	1.29	0.78	0.66	0.07	0.02	0.96	0.03	0.04	0.002
Na$_2$O	NA	0.74	0.73	0.46	0.91	0.71	0.03	0.10	0.003	2.91	0.00	0.00	1.67
MnO	0.07	0.06	0.05	0.03	0.05	0.05	0.08	0.10	0.10	0.04	0.29	0.37	0.03
ppm													
K	<5	11.6	26.2	<5	29.3	19.4	4.6	50.1	<5	401.7	<5	17.6	177
Sc	155	104	90.6	15.5	80.1	51.0	21.5	20.8	2.3	33.2	17.9	103	1.5
V	189	357	322	65.4	335	140	172	159	28.7	241	14.0	59.7	3.6
Co	17.9	45.9	38.8	18.2	35.6	30.0	63.6	75.3	74.0	40.1	54.2	42.4	NA
Ni	96.4	292	248	164	276	271	374	365	450	509	<20	<20	245
Rb	NA	0.24	0.34	0.006	0.12	0.13	0.20	0.37	0.15	1.9	0.010	0.61	NA
Sr	14.6	25.1	39.0	135.7	60.3	66.6	6.2	10.8	0.67	184.4	0.10	0.78	1260
Y	19.6	16.4	9.7	0.87	18.7	8.2	0.079	1.2	0.017	4.4	3.7	56.6	0.31
Zr	19.7	9.9	7.4	3.2	37.1	23.5	1.7	2.2	0.15	13.3	1.7	6.4	0.39
Nb	0.34	0.51	0.23	0.007	0.47	0.59	0.20	0.16	<0.002	0.27	<0.002	<0.002	0.015
Ba	0.060	1.1	1.1	0.064	0.88	0.70	0.12	0.74	0.17	10.4	0.011	0.068	<0.01
La	0.22	0.30	0.31	0.25	0.60	0.51	0.044	0.049	<0.002	0.80	0.025	0.013	0.27
Ce	0.97	1.5	1.3	0.98	2.7	2.0	0.082	0.15	0.002	3.2	0.039	0.009	0.52
Nd	2.2	2.4	1.9	1.2	4.8	3.5	0.064	0.24	<0.002	3.2	0.077	0.13	0.49
Sm	1.2	1.4	0.95	0.39	2.3	1.6	0.016	0.16	<0.002	1.2	0.12	0.47	0.10
Eu	0.38	0.39	0.34	0.14	0.48	0.36	0.009	0.051	<0.002	0.46	0.15	0.35	0.23
Gd	2.1	2.2	1.6	0.45	4.0	2.3	0.036	0.27	<0.002	1.4	0.38	2.7	0.082

(*Continued*)

Table 13.5 (Continued)

Sample	119-21	119-17	119-17	119-17	119-4	119-4	119-17	119-19	119-19	119-17	119-5N	119-19	119-5
Dy	3.2	3.0	2.0	0.29	4.1	2.1	0.028	0.28	0.004	1.1	0.60	8.6	0.065
Er	2.2	1.7	1.1	0.092	1.9	0.76	0.010	0.11	0.005	0.51	0.46	7.3	0.030
Yb	2.1	1.6	0.82	0.056	1.2	0.39	0.006	0.11	0.006	0.38	0.56	8.6	0.027
Lu	<0.002	0.20	0.094	0.003	0.13	0.039	0.002	0.016	0.002	0.050	0.082	1.3	0.004
Hf	0.41	0.44	0.39	0.20	2.6	1.8	0.061	0.19	0.003	0.70	0.062	0.14	NA
Ta	<0.002	0.030	0.027	<0.002	0.073	0.086	0.005	0.011	<0.002	0.014	<0.002	<0.002	NA
Pb	0.007	0.24	0.18	0.14	0.094	0.31	0.035	0.32	0.47	0.81	0.007	0.079	NA
Th	0.071	0.046	0.041	0.001	0.029	0.029	0.040	0.032	0.002	0.003	0.003	0.006	NA
U	0.002	0.009	0.010	<0.001	0.013	0.014	0.014	0.009	0.001	0.004	0.002	0.000	NA

NA, not analyzed.
[a]Domains indicated as new are fine-grained metamorphic crystals.
[b]"Pl" represents domain of altered plagioclase in the core of garnet.
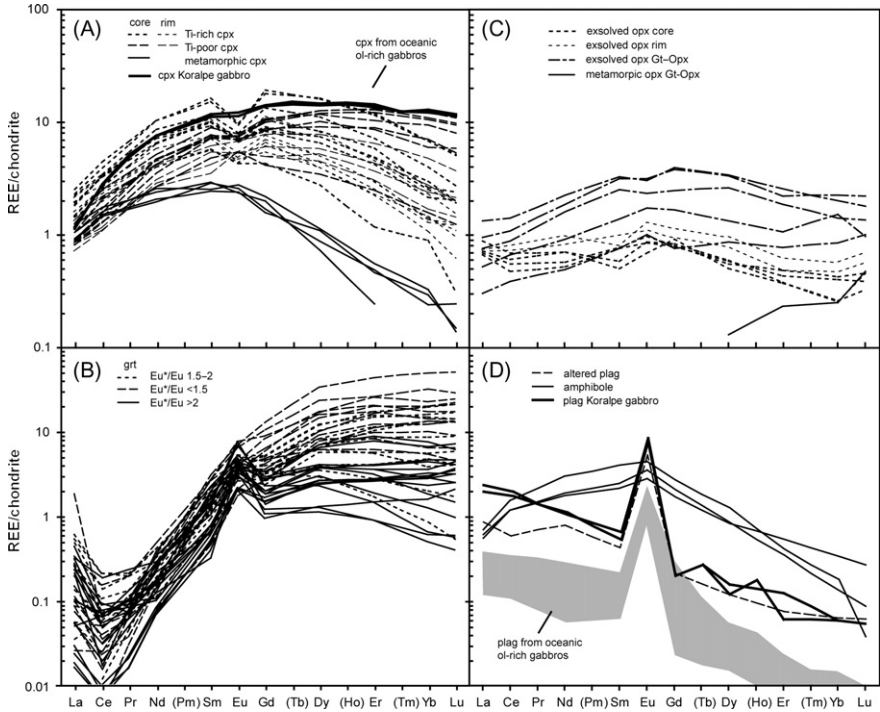
Figure 13.9 Mineral REE patterns normalized to chondrite (McDonough & Sun, 1995). (A) Clinopyroxene, (B) garnet, (C) orthopyroxene, and (D) amphibole and relict altered plagioclase. Cpx and Pl fields from oceanic olivine-rich gabbros from Drouin et al. (2009). Koralpe gabbro Cpx and Pl from Miller et al. (2007).

13.5.2.2 Orthopyroxene

Orthopyroxene was only measured in samples in which exsolved Opx was observed (119-17 and 119-19). In sample 119-17, REE patterns are rather irregular, probably because of low-REE contents (Figure 13.9C). They are flat compared to coexisting Cpx. TiO_2 contents are relatively high (0.45 wt% on average), which suggests that exsolved Opx is related to Ti-rich Cpx. In sample 119-19 (garnet orthopyroxenite), two generations of Opx exist: coarse-grained exsolved Opx and fine-grained metamorphic Opx, which forms most of the sample matrix. Exsolved Opx shows slightly humped patterns with low LREE and HREE and small negative Eu anomaly, not unlike patterns of Ti-rich Cpx in other samples (Figure 13.9A and C).

13.5.2.3 Garnet

Trace-element patterns in garnet appear compromised to variable degrees in nearly all samples because of garnet breakdown. Even in garnets that look relatively fresh, in high-magnification backscatter images garnets show a fine mesh pattern of
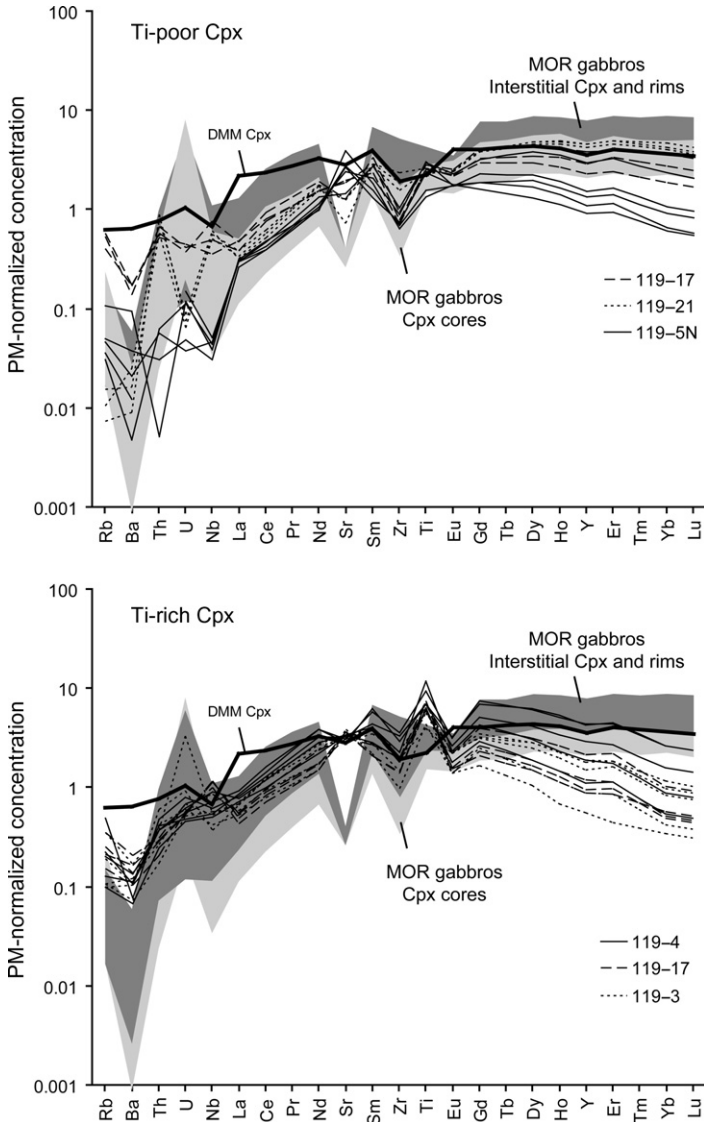
Figure 13.10 Clinopyroxene trace-element patterns normalized to primitive mantle (McDonough & Sun, 1995) for Ti-poor Cpx and Ti-rich Cpx. Fields indicated compositional range of crystal cores of cumulus and porphyritic Cpx (light gray) and Ti-rich rims of cumulus and porphyritic Cpx (>0.55 wt% TiO_2) and interstitial Cpx (dark gray) from olivine-rich gabbros and troctolites from the MAR (Drouin et al., 2009). Thick black line is the calculated composition of Cpx from DMM calculated from DMM, $D^{cpx/min}$, and modal composition of DMM (Workman & Hart, 2005). D values from Suhr et al. (1998) and Bedard (1994).

fractures and are patchy in appearance (Figure 13.2F). Nevertheless, several samples contain garnets that look reasonably fresh (119-3, 119-4, 119-5N, 119-6, 119-17). These have relatively flat HREE and Yb_N between 1 and 50, with steeply dipping L-MREE and with no or small positive Eu anomalies (Eu*/Eu <2; Table 13.5; Figure 13.9B). Many garnets show considerable enrichments in La, Ce, and Pr. Na_2O contents are very low (<0.01 wt%) as are TiO_2 contents (<0.04 wt%). Cr_2O_3 contents are low but variable (30−910 ppm). Sc contents are variable (8−100 ppm) as are Zr contents (3−22 ppm). Sr contents are low (0.1−1.2 ppm).

Samples 119-17, 119-6, 119-5N, and 119-21 also contain garnets with large positive Eu anomalies (Figure 13.9B) and low HREE contents (Yb_N 0.5−10). If these patterns are alteration features, then other trace elements were not affected, as they are similar to other garnets. We therefore regard the patterns as inherited from precursor plagioclase. Garnets with similar patterns have observed in coronitic garnet replacing plagioclase (Mazzucchelli et al., 1992).

13.5.2.4 Amphibole

Amphiboles are of metamorphic origin and show a slight depletion of LREE relative to MREE and a stronger depletion in HREE (Figure 13.9D). They are furthermore characterized by high Sr (140−150 ppm), Cr_2O_3 (0.34−0.77 wt%), and TiO_2 (∼0.4 wt%) contents.

13.5.2.5 Relict Former Plagioclase

Several samples contain garnets with core domains consisting of fine-grained, unidentified alteration minerals rich in CaO, Al_2O_3, and Na_2O (Figure 13.3A). Laser-ablation analysis of one of these domains indicates a Ca/Na ratio equivalent to plagioclase, with a An content of 85% as well as 180 ppm K and 1260 ppm Sr (Table 13.5). The latter is rather high for plagioclase, which suggests chemical transport during alteration or during metamorphic overgrowth by garnet. Nevertheless, its REE pattern is typical of plagioclase (Figure 13.9D), with high $(La/Yb)_N = 6$ and a strongly positive Eu anomaly (Eu/Eu* = 9). We interpret these domains to represent relicts of former anorthite-rich (An80-88) plagioclase.

13.6 Discussion

13.6.1 Protoliths

13.6.1.1 Cumulates or Residual Mantle Peridotites?

The average composition of Pohorje garnet peridotites, which straddles the lherzolite−olivine websterite boundary, is too enriched in CaO and Al_2O_3 for these rocks to be unmodified residual mantle peridotites, but they may have been impregnated by or reacted with migrating melts (Janák et al., 2006). However, the rocks contain

several features typical of cumulates, in particular those from the Prihovca locality. Rare earth element patterns are subparallel but show a wide range of REE contents and have positive Eu anomalies in the REE-poor samples, which gradually fade in samples with higher REE contents (Figure 13.6). This is typical for gabbroic cumulates, the bulk-rock composition of which reflects the relative amounts of their constituent minerals. Samples with low modal Cpx will inherit the low-REE contents and strong Eu anomalies from plagioclase, whereas increasing amounts of Cpx will increase REE contents and smooth the Eu anomaly. The composition of exsolved Cpx is also in support of a cumulate origin, as it has lower Al_2O_3 and higher TiO_2 than typical mantle Cpx (Elthon et al., 1992; Rivalenti et al., 1996) and is similar to Cpx from olivine gabbros and troctolites from the MAR (Elthon et al., 1992; Drouin et al., 2009).

Forsterite and NiO contents of olivine are consistent with a cumulate origin, as they are comparable to that of olivine-rich gabbros and troctolites (Elthon et al., 1992; Borghini et al., 2007; Drouin et al., 2009), although similar compositions can also be found in refertilized lherzolitic mantle (Suhr et al., 2008). The abundance of Ti-poor Cr-spinel with typical mantle compositions (Cr# $0.1-0.5$, Mg# $0.5-0.8$, <0.5 wt% TiO_2), however, is uncommon in ultramafic cumulates, in which Ti-rich spinel is more commonly observed (Dick & Bullen, 1984; Borghini & Rampone, 2007; Suhr et al., 2008; Drouin et al., 2009). Ti-poor spinel is not common in refertilized mantle either, as plagioclase peridotites mostly contain Ti-rich Cr-spinel (Dick & Bullen, 1984; Müntener & Piccardo, 2003). Note, however, that Ti-rich Cr-spinel was observed in more than half of the Pohorje garnet peridotite samples (Cr# $0.5-0.6$, Ti $0.5-2.8$ wt%) together with ilmenite and apatite. Remnants of altered plagioclase and cumulate textures of coarse-grained olivine and interstitial clinopyroxene further indicate an igneous protolith of Pohorje garnet peridotites (Figure 13.3).

Confirmation of the origin of these rocks comes from their PGE compositions. PGEs are highly compatible during mantle melting, with PPGE (Pd, Pt, Rh) being slightly less compatible than IPGE (Os, Ir, Ru). Hence, residual mantle rocks are rich in PGE, and their patterns change little during mantle melting apart from small depletions of PPGE relative to IPGE in depleted harzburgites (Hattori et al., 2010). Melts extracted from these peridotites, however, are poor in PGE and usually show fractionated patterns with primitive-mantle normalized PPGE > IPGE. The latter is what we observe for Pohorje garnet peridotites (Figure 13.11), which argues strongly against an origin as mantle peridotite. Therefore, we conclude that the protoliths of Pohorje garnet peridotites from the Prihovca locality were plagioclase-bearing ultramafic cumulates. The sample from Visole (VI01/04) is an exception, as its PGE contents are much closer to those of SBUC serpentinites and primitive mantle (Figure 13.11). Also its REE pattern is different from the other garnet peridotites, as it shows strongly depleted HREE and slightly enriched LREE. It also lacks exsolved clinopyroxene. The sample does, however, have a strong positive Eu anomaly, which suggests involvement of plagioclase in its history, similar to the other garnet peridotites. It thus probably represents a piece of mantle infiltrated by melt in the plagioclase stability field.
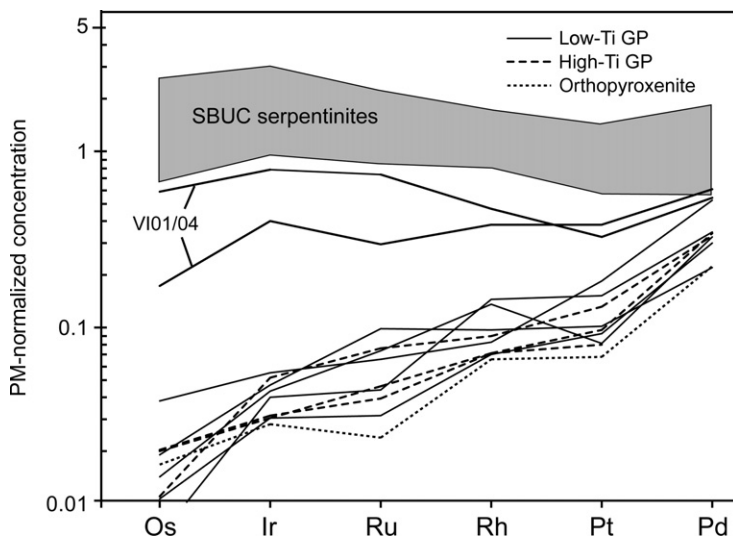
Figure 13.11 PGE contents normalized to primitive mantle for Pohorje garnet peridotites. Also indicated is the range of compositions from serpentinized harzburgites from the SBUC (De Hoog & Hattori, unpublished data). Primitive mantle values from McDonough and Sun (1995).

Coronitic troctolites were reported in the SBUC by Hinterlechner-Ravnik et al. (1991) and Visona et al. (1991), but their compositions are more evolved than the garnet peridotites in this study (Figure 13.4). Rocks with bulk chemical compositions similar to the Prihovca garnet peridotites are mela-olivine gabbros with garnet coronas around plagioclase from the Variscan Ötztal complex (Miller, 1974), and we regard the Pohorje rocks to be more intensely metamorphosed equivalents of a compositionally similar protolith. Olivine gabbros with An-rich plagioclase will form pyroxenites and peridotites upon metamorphism under eclogite-facies conditions following the reactions anorthite + olivine = garnet and albite + olivine = jadeite + enstatite (Figure 13.12). Note that no jadeite-rich Cpx has been observed in the samples presented in this study, but it was documented in coronitic metatroctolites (Hinterlechner-Ravnik et al., 1991; Visona et al., 1991) and in a few garnet peridotites from Pohorje as pseudomorphs after plagioclase together with kyanite and zoisite (Janák et al., 2008).

From the average bulk-rock composition (CIPW calculation), we estimate that the protolith of garnet peridotites from Prihovca contained ∼26% plagioclase with composition An82, ∼57% olivine with composition Fo87, ∼7% each diopsidic clinopyroxene and orthopyroxene, plus subordinate Cr-spinel and ilmenite. The CIPW composition is only an approximation as it ignores solid solutions, which is especially important in pyroxenes. Also, despite its presence in the CIPW norm composition, orthopyroxene of igneous origin was observed in only one of the samples (119-17). Therefore, we performed a least-squares calculation with a restored
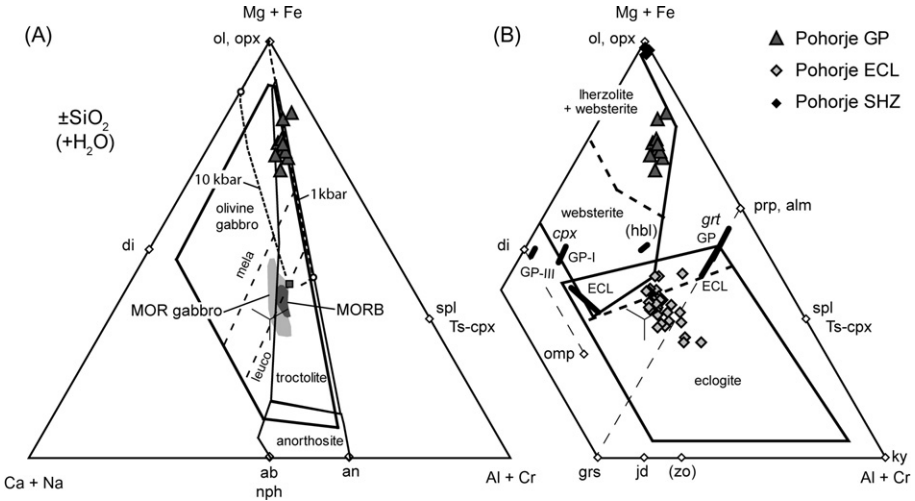
Figure 13.12 Ternary Ca + Na−Mg + Fe−Al + Cr diagrams of mafic and ultramafic rocks recalculated to mole fractions on a single cation basis projected from SiO_2. Main minerals are indicated with open diamonds (abbreviations from Whitney & Evans, 2010) with hydrous minerals between parentheses. Fields with rock names follow IUGS classification (Streckeisen, 1974). Note that fields may overlap because of solid solution between minerals, hence boundaries are approximate. (A) Low-pressure assemblages. Indicated are primary MORB (gray square (red diamond in web version); Herzberg & O'Hara, 2002) and fields of natural MOR basalts and gabbros (compiled from PETDB, http://www.petdb.org; Lehnert et al., 2000). Stippled lines (colored lines in the web version) indicate composition of aggregate solid during fractional crystallization of MORB at 1 and 10 kbar. At low pressure (blue line in web version), solids evolve from dunite to troctolite to olivine gabbro. At high pressure (red line in web version), Cpx crystallizes before plagioclase and the order becomes dunite−wehrlite−olivine gabbro. (B) High-pressure assemblages. Pohorje mafic and ultramafic rocks are plotted, as well as compositional ranges of Cpx, garnet, and hornblende. Olivine gabbro compositions above the di−prp join (most mela-olivine gabbros) will convert to garnet-bearing peridotites and pyroxenites upon eclogite-facies recrystallization, whereas those near the omp−prp join (leuco-olivine gabbros) will convert to eclogites.

Ti-poor Cpx composition (Table 13.4) without orthopyroxene and solved for the Fo and An contents of olivine and plagioclase. The result was similar to the CIPW calculation, with 26% plagioclase with composition An87, 64% olivine with composition Fo86, and 8% Cpx. The higher amount of olivine is mainly the result of excluding orthopyroxene. The mineral compositions and modes are similar to those of Ol-rich cumulates from the MAR (Drouin et al., 2009) and MORB-type cumulates in ophiolites (Borghini & Rampone, 2007).

A hybrid scenario between cumulate and melt infiltration has been proposed for some ultramafic rocks in gabbroic complexes on the MAR to explain Fo-rich olivine in plagioclase-rich cumulates (Suhr et al., 2008; Drouin et al., 2009). This model involves melt pockets that intruded into and reacted with depleted mantle

rocks, transforming them into olivine troctolites (Suhr et al., 2008; Drouin et al., 2009). A similar scenario may explain the unusual high Fo content of Pohorje garnet peridotites as well as the prevalence of low-Ti spinels with compositions similar to harzburgites from the SBUC (De Hoog et al., 2009). It is noteworthy that the Visole sample (VI01/04) has high NiO (0.28−0.35 wt%) for its relatively low Fo content (Fo88−89.5), and that samples from Prihovca (location 119) have a very narrow range of NiO (0.23−0.27) for a wide range of Fo contents (Fo86-90), consistent with reequilibration of the samples with evolved melts (Suhr et al., 2008).

The depletion of HREE in exsolved Cpx from Pohorje garnet peridotites (Figure 13.9) suggests growth of Cpx in the presence of garnet, which is at odds with an origin as plagioclase-bearing cumulates. These depletions can be observed in Ti-poor as well as Ti-rich Cpx and commonly show core to rim zoning. Only in sample 119-21 does Cpx show no HREE depletions, and we suspect that the variable HREE depletion of Cpx in other samples is the result of reequilibration during UHP metamorphism. Gabbros from the Ivrea zone with coronitic garnet replacing plagioclase commonly shows HREE depletions in Cpx (Mazzucchelli et al., 1992), whereas garnet-free samples do not. This indicates that REE patterns of Cpx are readily modified by small amounts of garnet growth.

The garnet orthopyroxenite (sample 119-19) contains many features typical of TiO_2-rich melts and lacks Fo-rich olivine and Ti-poor Cr-spinel. Orthopyroxene has Eu anomalies and REE patterns similar to Cpx in other samples. We therefore think that this rock may represent a vein of evolved melt expelled from the cumulate or migrating through it. Its unusual HREE-enriched REE pattern (Figure 13.7) suggests accumulation of garnet, which probably reflects chemical heterogeneity of the sample as it was coarse grained and rather small.

13.6.1.2 Protolith Petrogenesis and Tectonic Affinity

The chemical composition of cumulates cannot be used to infer their tectonic affinity directly, as it is significantly modified from the liquid composition by the crystal accumulation process. However, the composition of relict igneous clinopyroxene can be used with $D^{cpx/melt}$ values to estimate the composition of the parental liquid. In addition, mass-balance calculations of whole-rock and calculated mineral compositions and mineral modes can be used to constrain, if present, the fraction of trapped melt (TMF) in the cumulates (Bedard, 1994). Trapped melt will be highly enriched in incompatible elements compared to cumulate minerals and therefore strongly influence the whole-rock budget despite being volumetrically insignificant. Upon cooling of the cumulates, trapped melt will crystallize and form rims on cumulate minerals as well as interstitial minerals with evolved compositions (e.g., apatite, ilmenite) normally not expected in mafic rocks (Borghini & Rampone, 2007). In Pohorje samples, postcumulus overgrowths and chemical zoning have been obliterated by UHP metamorphism and later amphibolite-facies overprint, but intercumulus minerals are still preserved.

Exsolved Cpx in Pohorje garnet peridotites often shows evidence of partial reequilibration with metamorphic garnet; it is thus important to select Cpx with the

best-preserved igneous composition. Sample 119-21, a low-Ti sample, contains low-Ti clinopyroxenes with nearly flat HREE patterns, high Yb/La ratios, and little compositional variation and therefore represents the best estimate of igneous Cpx. In sample 119-4, a high-Ti sample, high-Ti clinopyroxene with only moderate HREE depletion is the best representative of more evolved igneous Cpx. Distribution coefficients were compiled from tholeiitic basalts in the literature (Bedard, 1994; Suhr et al., 1998). Calculations were performed using the estimated mineral modes from the previous section.

The calculated trace-element pattern of Ti-poor samples matches the observed composition well if assuming the presence of ∼2.5% trapped melt (Figure 13.13A). Typical features such as positive Eu and Sr anomalies and the relatively flat trace-element pattern are correctly replicated. This indicates that Ti-poor Cpx was in equilibrium with the other minerals (plagioclase, olivine), despite its interstitial texture (Figure 13.3). Crystallization of Cpx from the interstitial liquid would rapidly fractionate the composition of both Cpx and liquid, and Cpx would consequently be more evolved than the cumulus minerals. As this is not observed, the intercumulus liquid was probably interconnected and reequilibrated continuously with the main magma. This may also explain the lack of interstitial minerals such as ilmenite and apatite in Ti-poor samples.

The composition of the liquid in equilibrium with Ti-poor Cpx resembles that of N-MORB (Figure 13.11A). This is not surprising, as trace-element contents of Ti-poor Cpx are similar to those reported by Drouin et al. (2009) for primitive olivine-rich gabbros and troctolites from the MAR, apart from slight enrichments in alkali and earth alkaline elements (Figure 13.10A).

Significant differences in incompatible trace-element contents of Ti-poor Cpx were observed between samples, the origin of which is not clear (Figure 13.10A). One possibility is that trace-element patterns were modified by metamorphic reequilibration, as was observed for HREE. This would be most apparent for elements that show significantly different concentrations in metamorphic Cpx, which includes nearly all elements except LREE−MREE. However, different elements appear to behave differently: sample 119-17 has high incompatible elements (Rb to Nb in Figure 13.11A), whereas these are all low in 119-5N; and 119-21 has high Th and Nb, but low Rb, Ba, and U in addition to high Sr. Ti-rich Cpx does show comparable variations for these elements, despite having similar HREE depletions as Ti-poor Cpx. This suggests that differences may well be related to compositional differences of the melts from which Cpx crystallized.

Compositional modeling of Ti-rich samples is less straightforward. A scenario with larger amounts of Ti-poor TMF in the cumulate does not properly reproduce observed trace-element patterns (Figure 13.13B). However, Cpx in Ti-rich samples has a different composition than in Ti-poor samples, so the melt must have been more evolved. Using Ti-rich Cpx and melt does not greatly improve the results. Particularly Sr, Ba, and Rb show poor fits due to their high concentrations in Ti-rich Cpx. This suggests that plagioclase was not in equilibrium with Ti-rich Cpx. A more satisfactory fit is achieved by using the same cumulate minerals as in low-Ti samples and then adding TMF in equilibrium with Ti-rich Cpx
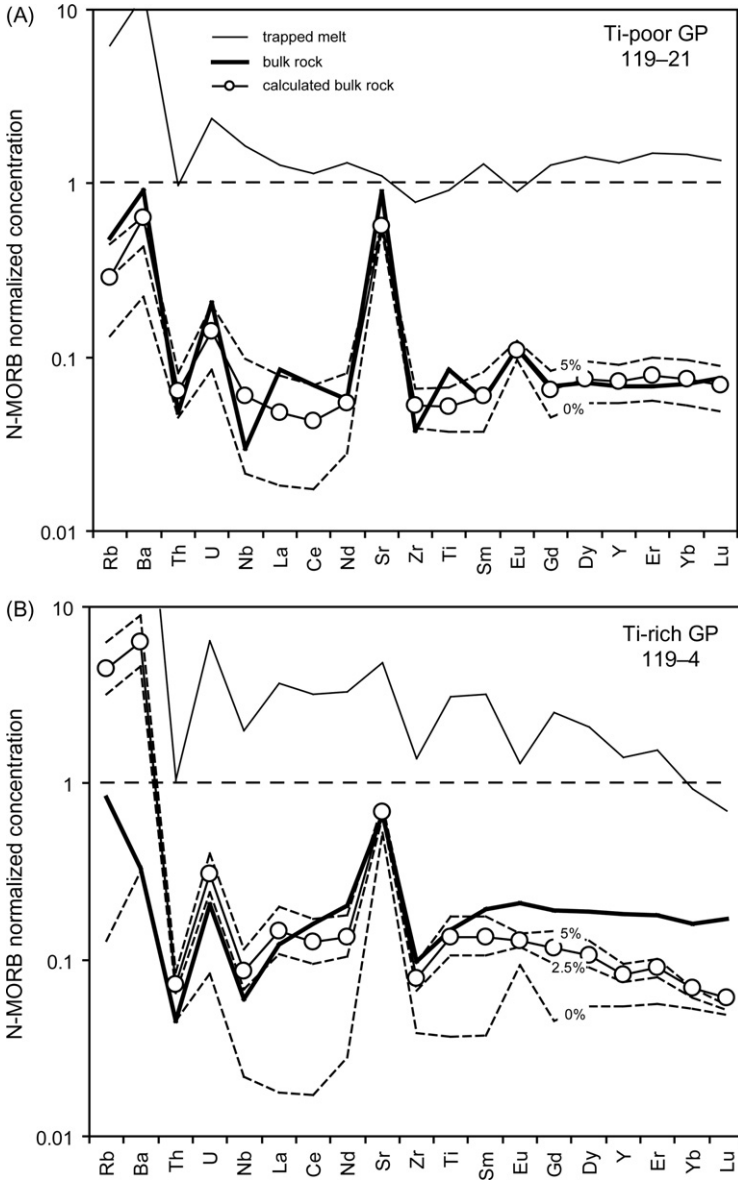
Figure 13.13 Calculated compositions of whole rock and melts in equilibrium with Cpx from Ti-rich and Ti-poor samples normalized to N-MORB (Sun & Mcdonough, 1989). Position of Sm has been changed to show more clearly the Eu anomaly which is obscured using the traditional element order. Lines with percentages are calculated whole-rock compositions for different fractions of trapped melt in the cumulate. For details, see Section 13.6.1.2. $D^{cpx/melt}$ after Suhr et al. (1998), $D^{plag/melt}$ and $D^{ol/melt}$ after Bedard (1994).

(Figure 13.13B). This scenario is plausible, seeing as Ti-rich melt is unlikely to be the source of the major cumulate minerals.

Melt in equilibrium with Ti-rich Cpx has a composition more fractionated than typical MORB (Figure 13.13). Compared to melt in equilibrium with Ti-poor Cpx, it is high in Ti, Sr, Zr, and LREE, has similar Eu and Y but lower Cr and Mg#. TiO_2-rich melt can be derived from the TiO_2-poor melt only by significant fractional crystallization. The most obvious scenario is that melt was trapped in between the cumulate minerals and no longer reequilibrated with the main magma, but continued to evolve during cooling, eventually crystallizing Ti-rich Cpx, Ti-rich chromite, ilmenite, and apatite. This explains the increased contents of TiO_2 and other incompatible elements in these samples. Strong negative Eu anomalies support continued crystallization in the presence of plagioclase with the melt being increasingly depleted. Cpx with compositions similar to TiO_2-rich Cpx in Pohorje garnet peridotites is found as interstitial clinopyroxene in olivine-rich plagioclase-bearing cumulates (Borghini & Rampone, 2007; Drouin et al., 2009). In contrast to Ti-poor Cpx, Ti-rich Cpx has highly variable Ti contents. Large variations in TiO_2 contents with little accompanying change in Mg# is considered the result of postcumulus crystallization (Borghini & Rampone, 2007); this is also observed in Cpx here.

The fit for Ba and Rb remains poor. As most Ba and Rb contents in Cpx from Ti-poor samples are also high (but not in 119-21, used for modeling), this suggests reequilibration during metamorphism. Ba and Sr are mobile in fluids, and Cpx is commonly partially amphibolitized along exsolution lamellae (Figure 13.2D). Hence, Ba and Rb were probably transported into Cpx along with the metamorphic fluid.

13.6.2   Geodynamic Implications

In the previous sections it was established that the protoliths of most of the Pohorje garnet peridotites were igneous cumulates. Their presence within the SBUC indicates that the rocks crystallized in a magma chamber emplaced within lithospheric mantle. The large amounts of plagioclase and interstitial character of Cpx in relict cumulate textures (Figure 13.3) suggest that the protoliths crystallized at pressures below ~5 kbar (Figure 13.12), as plagioclase is replaced by clinopyroxene as the second crystallizing phase (after olivine) at higher pressures (Villiger et al., 2007). This implies a shallow position of the depleted mantle rocks of the SBUC at the time of intrusion of the olivine gabbros. Shallow mantle is typically exhumed at slow-spreading magma-poor ridges or at passively rifted continental margins (Dick et al., 1984; Müntener & Piccardo, 2003) and commonly contains primitive cumulates (Rivalenti et al., 1981; Borghini et al., 2007; Drouin et al., 2009).

In addition to garnet peridotites, the SBUC hosts eclogites, including several larger bodies at its contact with overlying continental crust units (Kirst et al., 2010). The geochemical composition of these eclogites supports a genetic link with the garnet peridotites, as trace-element patterns are similar (Figure 13.7), and the

major element composition of garnet peridotites can be reproduced by adding olivine to eclogites (Figure 13.12). Hence, garnet peridotites are the more primitive equivalents of eclogites. Eclogites within the SBUC are metagabbros of oceanic affinity (Sassi et al., 2004; Miller et al., 2005), whereas the SBUC itself is thought to be a former piece of residual oceanic mantle based on its geochemical similarities to abyssal peridotites (De Hoog et al., 2009).

Several scenarios have been proposed to explain the presence of mantle rocks and associated mafic rocks of oceanic affinity in Pohorje. Janák et al. (2006) suggested that the garnet peridotites were derived from the overlying mantle during deep subduction of continental crust. This scenario was adopted for the complete SBUC by De Hoog et al. (2009), who determined that it was most likely a remnant of oceanic mantle. As subduction was intracontinental (Janák et al., 2004), the presence of oceanic mantle in Pohorje is unexpected; therefore De Hoog et al. (2009) proposed a scenario in which continental subduction progressed deeply enough to be juxtaposed to remnants of subducted Meliata oceanic lithosphere. As an alternative, De Hoog et al. (2009) considered that mantle was incorporated in the crust during Permian rifting. Kirst et al. (2010) support the latter scenario based on structural considerations and argue that mantle and overlying continental crust were subducted as a coherent unit. This would imply that the SBUC was derived from subcontinental lithosphere and partially exhumed during continental rifting.

Many ophiolitic complexes have been preserved in the Western and Central Alps related to continental rifting and formation of oceanic basins, the geological features of which can be compared with the Pohorje region. On the continental side of continent−ocean transition zones, exhumed mantle commonly has a subcontinental origin and often contains small volumes of genetically unrelated MORB-type material (Desmurs et al., 2002; Müntener et al., 2004; Tribuzio et al., 2004; Borghini et al., 2007; Montanini et al., 2008). Exhumed mantle from the ocean side is often plagioclase bearing and represents depleted mantle extensively refertilized by N-MORB-type melts (Müntener & Piccardo, 2003; Müntener et al., 2004, 2010).

Strongly depleted mantle is uncommon in the continental part of continent−ocean transition zones. It has nevertheless been found off the coast of Newfoundland, where it was suggested that sub-arc mantle must be present under the continent (Müntener & Manatschal, 2006). An origin within continental rifting for the SBUC would require strongly depleted mantle to be present beneath Pohorje during the Permian, but this is unlikely considering that mantle xenoliths in the region show no signs of extensive depletion (Vaselli et al., 1996) and no other occurrences of strongly depleted ultramafic rocks from that time have been found in the area.

Alternatively, the SBUC may represent a fragment of mantle from the ocean side of a continent−ocean transition zone, as strongly depleted mantle material similar to the SBUC has been found in such settings (Rampone et al., 1998; Müntener et al., 2010). In this scenario, continental rifting in Pohorje must have progressed to or beyond incipient oceanization. This is consistent with Nd and Sr isotope data from Pohorje eclogites, which indicate interaction with seawater (Miller et al., 2005), but inconsistent with the lack of oceanic sediments in the

Eastern Alps before opening of the Meliata ocean around 237 Ma (Froitzheim, personal communication).

We cannot exclude that the SBUC is part of an older ophiolitic complex emplaced within the continental crust before the Permian. The protoliths of the garnet peridotites may have been part of the ophiolite complex at the time of emplacement, or, considering their similarities with mafic rocks elsewhere with the Central Austroalpine, were the product of magmatism during Permian continental rifting. Complexes with similarly depleted harzburgitic compositions occur elsewhere within the Lower Central Austroalpine but, in contrast to the SBUC, these show evidence of prolonged, (pre-)Variscan histories (Faryad et al., 2002; Melcher & Meisel, 2004). Future work on the protolith ages of the different mafic and ultramafic units may provide more definite constraints on the origin of the SBUC and Pohorje garnet peridotites.

13.7   Conclusions

Garnet peridotites from the SBUC in Pohorje, Slovenia, are former low-pressure, plagioclase-bearing ultramafic cumulates metamorphosed during Eo-alpine intracontinental subduction. The shallow level of intrusion of the garnet peridotite protolith indicates that the SBUC mantle rocks were (partially) exhumed at the time of magma emplacement. Remnants of igneous minerals allow identification of the composition of melts from which the cumulates crystallized. The rocks are of oceanic affinity and form the more primitive equivalent to associated eclogitized metagabbros within the SBUC and surrounding continental crust. The oceanic affinity of mafic and ultramafic units in Pohorje indicates a depleted asthenospheric mantle source. The two most likely scenarios of formation of the SBUC and garnet peridotites are (1) emplacement within the continental crust during intracontinental subduction, in which case the SBUC most likely represents a remnant of the lithosphere beneath the subducted Meliata ocean floor or (2) emplacement within the continental crust as an ophiolite complex, probably before the Permian. To resolve these problems additional geochronological constraints are needed.

Acknowledgments

References

Barnes, S.J., 2000. Chromite in komatiites, 2. Modification during greenschist to mid-amphibolite facies metamorphism. J. Petrol. 41, 387−409.

Bedard, J.H., 1994. A procedure for calculating the equilibrium distribution of trace-elements among the minerals of cumulate rocks, and the concentration of trace-elements in the coexisting liquids. Chem. Geol. 118, 143−153.

Borghini, G., Rampone, E., 2007. Postcumulus processes in oceanic-type olivine-rich cumulates: the role of trapped melt crystallization versus melt/rock interaction. Contrib. Mineral. Petrol. 154, 619−633.

Borghini, G., Rampone, E., Crispini, L., De Ferrari, R., Godard, M., 2007. Origin and emplacement of ultramafic−mafic intrusions in the Erro-Tobbio mantle peridotite (Ligurian Alps, Italy). Lithos 94, 210−229.

Bruand, E., Stuwe, K., Proyer, A., 2010. Pseudosection modelling for a selected eclogite body from the Koralpe (Hohl), Eastern Alps. Miner. Petrol. 99, 75−87.

Brueckner, H.K., Medaris, L.G., 2000. A general model for the intrusion and evolution of "mantle" garnet peridotites in high-pressure and ultra-high-pressure metamorphic terranes. J. Metamorph. Geol. 18, 123−133.

Carswell, D.A., 1986. The metamorphic evolution of Mg−Cr Type Norwegian garnet peridotites. Lithos 19, 279−297.

Chopin, C., 2003. Ultrahigh-pressure metamorphism: tracing continental crust into the mantle. Earth Planet. Sci. Lett. 212, 1−14.

De Hoog, J.C.M., Janák, M., Vrabec, M., Froitzheim, N., 2009. Serpentinised peridotites from an ultrahigh-pressure terrane in the Pohorje Mts. (Eastern Alps, Slovenia): geochemical constraints on petrogenesis and tectonic setting. Lithos 109, 209−222.

De Hoog, J.C.M., Gall, L., Cornell, D.H., 2010. Trace-element geochemistry of mantle olivine and application to mantle petrogenesis and geothermobarometry. Chem. Geol. 270, 196−215.

Desmurs, L., Müntener, O., Manatschal, G., 2002. Onset of magmatic accretion within a magma-poor rifted margin: a case study from the Platta ocean−continent transition, eastern Switzerland. Contrib. Mineral. Petrol. 144, 365−382.

Dick, H.J.B., Bullen, T., 1984. Chromian spinel as a petrogenetic indicator in abyssal and alpine-type peridotites and spatially associated lavas. Contrib. Mineral. Petrol. 86, 54−76.

Dick, H.J.B., Fisher, R.L., Bryan, W.B., 1984. Mineralogic variability of the uppermost mantle along mid-ocean ridges. Earth Planet. Sci. Lett. 69, 88−106.

Drouin, M., Godard, M., Ildefonse, B., Bruguier, O., Garrido, C.J., 2009. Geochemical and petrographic evidence for magmatic impregnation in the oceanic lithosphere at Atlantis Massif, Mid-Atlantic Ridge (IODP Hole U1309D, 30 degrees N). Chem. Geol. 264, 71−88.

Elthon, D., Stewart, M., Ross, D.K., 1992. Compositional trends of minerals in oceanic cumulates. J. Geophys. Res. [Solid Earth] 97, 15189−15199.

Faryad, S.W., Henjes-Kunst, F., 1997. Petrological and K-Ar and Ar-40-Ar-39 age constraints for the tectonothermal evolution of the high-pressure Meliata unit, Western Carpathians (Slovakia). Tectonophysics 280, 141−156.

Faryad, S.W., Melcher, F., Hoinkes, G., Puhl, J., Meisel, T., Frank, W., 2002. Relics of eclogite facies metamorphism in the Austroalpine basement, Hochgrossen (Speik complex), Austria. Mineral. Petrol. 74, 49−73.

Fodor, L.I., Jelen, B., Marton, E., 2002. Connection of Neogene basin formation, magmatism and cooling of metamorphics in NE Slovenia. Geol. Carpath. 53, 199−201.

Fodor, L.I., Balogh, K., Dunkl, I., 2003. Structural evolution and exhumation of the Pohorje-Kozjak Mts., Slovenia. Ann. Univ. Scient. Budapest. Sect. Geol. 35, 118−119.

Frisch, W., 1979. Tectonic progradation and plate tectonic evolution of the Alps. Tectonophysics 60, 121−139.

Godard, M., Awaji, S., Hansen, H., Hellebrand, E., Brunelli, D., Johnson, K., et al., 2009. Geochemistry of a long in-situ section of intrusive slow-spread oceanic lithosphere: results from IODP site U1309 (Atlantis Massif, 30 degrees N Mid-Atlantic-Ridge). Earth Planet. Sci. Lett. 279, 110−122.

Hattori, K.H., Guillot, S., Saumur, B.M., Tubrett, M.N., Vidal, O., Morfin, S., 2010. Corundum-bearing garnet peridotite from northern Dominican Republic: a metamorphic product of an arc cumulate in the Caribbean subduction zone. Lithos 114, 437−450.

Herzberg, C., O'Hara, M.J., 2002. Plume-associated ultramafic magmas of Phanerozoic age. J. Petrol. 43, 1857−1883.

Hinterlechner-Ravnik, A., Sassi, F.P., Visona, D., 1991. The Austridic eclogites, metabasites and metaultrabasites from the Pohorje area (eastern Alps, Yugoslavia): 2. The metabasites and metaultrabasites, and concluding considerations. Rendiconti Fisiche Accademia Lincei 2, 175−190.

Janák, M., Froitzheim, N., Luptak, B., Vrabec, M., Ravna, E.J.K., 2004. First evidence for ultrahigh-pressure metamorphism of eclogites in Pohorje, Slovenia: tracing deep continental subduction in the Eastern Alps. Tectonics 23, Tc5014.

Janák, M., Froitzheim, N., Vrabec, M., Ravna, E.J.K., De Hoog, J.C.M., 2006. Ultrahigh-pressure metamorphism and exhumation of garnet peridotite in Pohorje, Eastern Alps. J. Metamorph. Geol. 24, 19−31.

Janák, M., Vrabec, M., Froitzheim, N., De Hoog, J.C.M., 2008. Omphacite-bearing garnet from Pohorje, Eastern Alps: constraints on the protoliths and UHP metamorphism of mantle-derived rocks, 33rd International Geological Congress, Oslo, Norway.

Janák, M., Cornell, D., Froitzheim, N., De Hoog, J.C.M., Broska, I., Vrabec, M., et al., 2009. Eclogite-hosting metapelites from the Pohorje Mountains (Eastern Alps): P-T evolution, zircon geochronology and tectonic implications. Eur. J. Mineral. 21, 1191−1212.

Kirst, F., Sandmann, S., Nagel, T., Froitzheim, N. and Janak, M., 2010. Tectonic evolution of the southeastern part of the Pohorje Mountains (Eastern Alps, Slovenia). Geol. Carpath. 61, 451−461.

Kurz, W., Fritz, H., 2003. Tectonometamorphic evolution of the Anstroalpine Nappe Complex in the central Eastern Alps—Consequences for the Eo-Alpine evolution of the Eastern Alps. Int. Geol. Rev. 45, 1100−1127.

Lehnert, K., Su, Y., Langmuir, C., Sarbas, B., Nohl, U., 2000. A global geochemical database structure for rocks. Geochem. Geophy. Geosyst. 1, doi:10.1029/1999GC000026.

Maluski, H., Rajlich, P., Matte, P., 1993. Ar-40-Ar-39 dating of the inner Carpathians variscan basement and Alpine mylonitic overprinting. Tectonophysics 223, 313−337.

Mazzucchelli, M., Rivalenti, G., Vannucci, R., Bottazzi, P., Ottolini, L., Hofmann, A.W., et al., 1992. Trace-element distribution between clinopyroxene and garnet in gabbroic rocks of the deep crust—an ion microprobe study. Geochim. Cosmochim. Acta 56, 2371−2385.

McDonough, W.F., Sun, S.S., 1995. The composition of the earth. Chem. Geol. 120, 223−253.

Melcher, F., Meisel, T., 2004. A metamorphosed early Cambrian crust−mantle transition in the Eastern Alps, Austria. J. Petrol. 45, 1689−1723.

Miller, C., 1974. Reaction rims between olivine and plagioclase in metaperidotites, Otztal-Alps, Austria. Contrib. Mineral. Petrol. 43, 333−342.

Miller, C., Konzett, J., 2005. Comment on "First evidence for ultrahigh-pressure metamorphism of eclogites in Pohorje, Slovenia: tracing deep continental subduction in the eastern Alps" by Marian Janak et al. Tectonics 24, Tc6010.

Miller, C., Mundil, R., Thöni, M., Konzett, J., 2005. Refining the timing of eclogite metamorphism: a geochemical, petrological, Sm-Nd and U-Pb case study from the Pohorje Mountains, Slovenia (Eastern Alps). Contrib. Mineral. Petrol. 150, 70−84.

Miller, C., Thöni, M., 1995. Origin of eclogites from the Austroalpine Otztal basement (Tirol, Austria)—Geochemistry and Sm−Nd vs Rb−Sr isotope systematics. Chem. Geol. 122, 199−225.

Miller, C., Thöni, M., 1997. Eo-Alpine eclogitisation of Permian MORB-type gabbros in the Koralpe (Eastern Alps, Austria): new geochronological, geochemical and petrological data. Chem. Geol. 137, 283−310.

Miller, C., Zanetti, A., Thöni, M., Konzett, J., 2007. Eclogitisation of gabbroic rocks: redistribution of trace elements and Zr in rutile thermometry in an Eo-Alpine subduction zone (Eastern Alps). Chem. Geol. 239, 96−123.

Mioč, P., Žnidarčič, M., 1977. Geological Map of SFRJ. Geological Survey, Ljubljana, Slovenia.

Montanini, A., Tribuzio, R., Vernia, L., 2008. Petrogenesis of basalts and gabbros transition (external Liguride from an ancient continent−ocean ophiolites, Northern Italy). Lithos 101, 453−479.

Müntener, O., Manatschal, G., 2006. High degrees of melt extraction recorded by spinel harzburgite of the Newfoundland margin: the role of inheritance and consequences for the evolution of the southern North Atlantic. Earth Planet. Sci. Lett. 252, 437−452.

Müntener, O., Piccardo, G.B., 2003. Melt migration in ophiolitic peridotites: the message from Alpine−Apennine peridotites and implications for embryonic ocean basins. In: Dilek, Y., Robertson, P.T. (Eds.), Ophiolites in Earth History. Geological Society of London, London, pp. 69−89. Special Publications.

Müntener, O., Pettke, T., Desmurs, L., Meier, M., Schaltegger, U., 2004. Refertilization of mantle peridotite in embryonic ocean basins: trace element and Nd isotopic evidence and implications for crust−mantle relationships. Earth Planet. Sci. Lett. 221, 293−308.

Müntener, O., Manatschal, G., Desmurs, L., Pettke, T., 2010. Plagioclase peridotites in ocean−continent transitions: refertilized mantle domains generated by melt stagnation in the shallow mantle lithosphere. J. Petrol. 51, 255−294.

Pearce, N.J.G., Perkins, W.T., Westgate, J.A., Gorton, M.P., Jackson, S.E., Neal, C.R., et al., 1997. A compilation of new and published major and trace element data for NIST SRM 610 and NIST SRM 612 glass reference materials. Geostand. Newslett. 21, 115−144.

Rampone, E., Hofmann, A.W., Raczek, I., 1998. Isotopic contrasts within the internal Liguride ophiolite (N. Italy): the lack of a genetic mantle−crust link. Earth Planet. Sci. Lett. 163, 175−189.

Rivalenti, G., Garuti, G., Rossi, A., Siena, F., Sinigoi, S., 1981. Existence of different peridotite types and of a layered igneous complex in the Ivrea Zone of the Western Alps. J. Petrol. 22, 127−153.

Rivalenti, G., Vannucci, R., Rampone, E., Mazzucchelli, M., Piccardo, G.B., Piccirillo, E.M., et al., 1996. Peridotite clinopyroxene chemistry reflects mantle processes rather than continental versus oceanic settings. Earth Planet. Sci. Lett. 139, 423−437.

Sassi, R., Mazzoli, C., Miller, C., Konzett, E., 2004. Geochemistry and metamorphic evolution of the Pohorje Mountain eclogites from the easternmost Austroalpine basement of the Eastern Alps (Northern Slovenia). Lithos 78, 235−261.

Schmid, S.M., Fugenschuh, B., Kissling, E., Schuster, R., 2004. Tectonic map and overall architecture of the Alpine orogen. Eclogae Geol. Helv. 97, 93−117.

Schuster, R., Koller, F., Hoeck, V., Hoinkes, G., Bousquet, R., 2004. Explanatory notes to the map: metamorphic structure of the Alps—Metamorphic evolution of the Eastern Alps. Mitt. Österreich. Mineral. Ges. 149, 175−199.

Schuster, R., Stüwe, K., 2008. Permian metamorphic event in the Alps. Geology 36, 603−606.

Shervais, J.W., 1982. Ti−V plots and the petrogenesis of modern and ophiolitic lavas. Earth Planet. Sci. Lett. 59, 101−118.

Streckeisen, A., 1974. Classification and nomenclature of plutonic rocks recommendations of the IUGS subcommission on the systematics of igneous rocks. Geol. Rundsch. 63, 773−785.

Suhr, G., Seck, H.A., Shimizu, N., Gunther, D., Jenner, G., 1998. Infiltration of refractory melts into the lowermost oceanic crust: evidence from dunite- and gabbro-hosted clinopyroxenes in the Bay of Islands ophiolite. Contrib. Mineral. Petrol. 131, 136−154.

Suhr, G., Hellebrand, E., Johnson, K., Brunelli, D., 2008. Stacked gabbro units and intervening mantle: a detailed look at a section of IODP Leg 305, Hole U1309D. Geochem. Geophy. Geosyst. 9, Q10007.

Sun, S.S., Mcdonough, W.F., 1989. Chemical and isotopic systematics of oceanic basalts; implications for mantle composition and processes. In: Saunders, A.D., Norry, M.J. (Eds.), Magmatism in the Ocean Basins. Geological Society of London, London, pp. 313−345.

Thöni, M., 2002. Sm−Nd isotope systematics in garnet from different lithologies (Eastern Alps): age results and an evaluation of potential problems for garnet Sm−Nd chronometry. Chem. Geol. 185, 255−281.

Thöni, M., Jagoutz, E., 1992. Some new aspects of dating eclogites in orogenic belts—Sm−Nd, Rb−Sr, and Pb−Pb isotopic results from the Austroalpine Saualpe and Koralpe type-locality (Carinthia Styria, Southeastern Austria). Geochim. Cosmochim. Acta 56, 347−368.

Thoni, M., Jagoutz, E., 1993. Isotopic constraints for Eo-Alpine high-P metamorphism in the Austroalpine Nappes of the Eastern Alps—Bearing on Alpine orogenesis. Schweiz. Mineral. Petrogr. Mitt. 73, 177−189.

Thöni, M., Miller, C., 1996. Garnet Sm−Nd data from the Saualpe and the Koralpe (eastern Alps, Austria): chronological and P−T constraints on the thermal and tectonic history. J. Metamorph. Geol. 14, 453−466.

Tribuzio, R., Thirlwall, M.F., Vannucci, R., 2004. Origin of the gabbro-peridotite association from the Northern Apennine ophiolites (Italy). J. Petrol. 45, 1109−1124.

Vaselli, O., Downes, H., Thirlwall, M.F., Vannucci, R., Coradossi, N., 1996. Spinel-peridotite xenoliths from Kapfenstein (Graz Basin, Eastern Austria): a geochemical and petrological study. Mineral. Petrol. 57, 23−50.

Villiger, S., Müntener, O., Ulmer, P., 2007. Crystallization pressures of mid-ocean ridge basalts derived from major element variations of glasses from equilibrium and fractional crystallization experiments. Journal of Geophysical Research-Solid Earth 112, B01202, 18 pp. doi:10.1029/2006JB004342.

Visona, D., Hinterlechner-Ravnik, A., Sassi, F.P., 1991. Geochemistry and crustal P−T polymetamorphic path of the mantle-derived rocks from the Pohorje area (Austrides, Eastern Alps, Slovenia). Miner. Slov. 23, 515−525.

Vrabec, M., 2004. High-pressure to ultrahigh-pressure metamorphism of Pohorje eclogites. M.Sc. Thesis, University of Ljubljana, Slovenia, Ljubljana.

Vrabec, M., 2007. Petrology of ultrahigh-pressure metamorphic rocks from Pohorje. Ph.D. Thesis, University of Ljubljana, Slovenia, Ljubljana.

Whitney, D.L., Evans, B.W., 2010. Abbreviations for names of rock-forming minerals. Am. Mineral. 95, 185−187.

Workman, R.K., Hart, S.R., 2005. Major and trace element composition of the depleted MORB mantle (DMM). Earth Planet. Sci. Lett. 231, 53−72.